



LAWRENCE  
LIVERMORE  
NATIONAL  
LABORATORY

# Dispersion of Radionuclides and Exposure Assessment in Urban Environments: a joint CEA and LLNL report

L. Glascoe, A. Gowardhan, K. Lennox, M. Simpson, K.  
Yu, P. Armand, C. Duchenne, F. Mariotte, X. Pectorin

February 17, 2015

## **Disclaimer**

---

This document was prepared as an account of work sponsored by an agency of the United States government. Neither the United States government nor Lawrence Livermore National Security, LLC, nor any of their employees makes any warranty, expressed or implied, or assumes any legal liability or responsibility for the accuracy, completeness, or usefulness of any information, apparatus, product, or process disclosed, or represents that its use would not infringe privately owned rights. Reference herein to any specific commercial product, process, or service by trade name, trademark, manufacturer, or otherwise does not necessarily constitute or imply its endorsement, recommendation, or favoring by the United States government or Lawrence Livermore National Security, LLC. The views and opinions of authors expressed herein do not necessarily state or reflect those of the United States government or Lawrence Livermore National Security, LLC, and shall not be used for advertising or product endorsement purposes.

This work performed under the auspices of the U.S. Department of Energy by Lawrence Livermore National Laboratory under Contract DE-AC52-07NA27344.



# Dispersion of Radionuclides and Exposure Assessment in Urban Environments

A Joint LLNL – CEA Report on the Common Table Top Exercise 17-18 June 2014  
 LLNL-TR-667436  
 INT -RET- RBC DET 15000067 A – CEA/DIF/DASE/SRCE/011/2015/DR

## Authors:

**Patrick Armand, Christophe Duchenne,  
 Frédéric Mariotte, Xavier Pectorin**

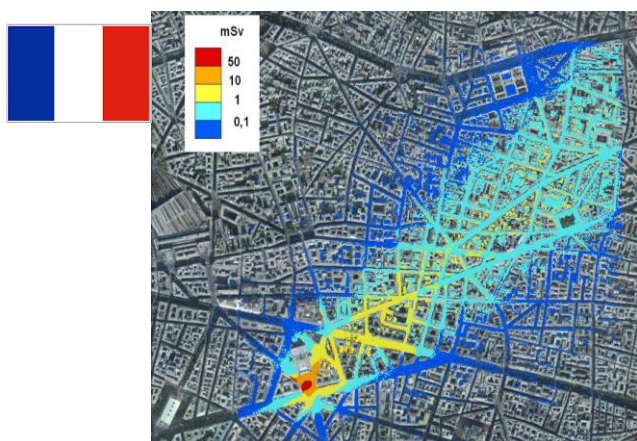
Commissariat à l'Énergie Atomique  
 et aux énergies alternatives, France

**Lee Glascoe, Akshay Gowardhan,  
 Kristin Lennox, Matthew Simpson,  
 Kristen Yu**

Lawrence Livermore National Laboratory  
 Livermore, California, USA

## Date:

19<sup>th</sup> of December 2014



**ABSTRACT:** In the interest of promoting the international exchange of technical expertise, the US Department of Energy's Office of Emergency Operations (NA-40) and the French Commissariat à l'Energie Atomique et aux énergies alternatives (CEA) requested that the National Atmospheric Release Advisory Center (NARAC) of Lawrence Livermore National Laboratory (LLNL) in Livermore, California host a joint table top exercise with experts in emergency management and atmospheric transport modeling. In this table top exercise, LLNL and CEA compared each other's flow and dispersion models. The goal of the comparison is to facilitate the exchange of knowledge, capabilities, and practices, and to demonstrate the utility of modeling dispersal at different levels of computational fidelity. Two modeling approaches were examined, a regional scale modeling approach, appropriate for simple terrain and/or very large releases, and an urban scale modeling approach, appropriate for small releases in a city environment. This report is a summary of LLNL and CEA modeling efforts from this exercise. Two different types of LLNL and CEA models were employed in the analysis: urban-scale models (Aeolus CFD at LLNL/NARAC and Parallel-Micro-SWIFT-SPRAY, PMSS<sup>1</sup>, at CEA) for analysis of a 5,000 Ci radiological release and Lagrangian Particle Dispersion Models (LODI at LLNL/NARAC and PSPRAY at CEA) for analysis of a much larger (500,000 Ci) regional radiological release. Two densely-populated urban locations were chosen: Chicago with its high-rise skyline and gridded street network and Paris with its more consistent, lower building height and complex unaligned street network. Each location was considered under early summer daytime and nighttime conditions. Different levels of fidelity were chosen for each scale: (1) lower fidelity mass-consistent diagnostic, intermediate fidelity Navier-Stokes RANS models, and higher fidelity Navier-Stokes LES for urban-scale analysis, and (2) lower-fidelity single-profile meteorology versus higher-fidelity three-dimensional gridded weather forecast for regional-scale analysis. Tradeoffs between computation time and the fidelity of the results are discussed for both scales. LES, for example, requires nearly 100 times more processor time than the mass-consistent diagnostic model or the RANS model, and seems better able to capture flow entrainment behind tall buildings. As anticipated, results obtained by LLNL and CEA at regional scale around Chicago and Paris look very similar in terms of both atmospheric dispersion of the radiological release and total effective dose. Both LLNL and CEA used the same meteorological data, Lagrangian particle dispersion models, and the same dose coefficients. LLNL and CEA urban-scale modeling results show consistent phenomenological behavior and predict similar impacted areas even though the detailed 3D flow patterns differ, particularly for the Chicago cases where differences in vertical entrainment behind tall buildings are particularly notable. Although RANS and LES (LLNL) models incorporate more detailed physics than do mass-consistent diagnostic flow models (CEA), it is not possible to reach definite conclusions about the prediction fidelity of the various models as experimental measurements were not available for comparison<sup>2</sup>. Stronger conclusions about the relative performances of the models involved and evaluation of the tradeoffs involved in model simplification could be made with a systematic benchmarking of urban-scale modeling. This could be the purpose of a future US / French collaborative exercise.

---

<sup>1</sup> Note that all acronyms are defined in Section 13.

<sup>2</sup> It is worth noting that the LLNL Aeolus and the CEA PMSS models have been validated to data collected in Oklahoma City in 2003.

**Disclaimer and Auspices:** This document was prepared as an account of work sponsored by an agency of the United States government. Neither the United States government nor Lawrence Livermore National Security, LLC, nor any of their employees makes any warranty, expressed or implied, or assumes any legal liability or responsibility for the accuracy, completeness, or usefulness of any information, apparatus, product, or process disclosed, or represents that its use would not infringe privately owned rights. Reference herein to any specific commercial product, process, or service by trade name, trademark, manufacturer, or otherwise does not necessarily constitute or imply its endorsement, recommendation, or favoring by the United States government or Lawrence Livermore National Security, LLC. The views and opinions of authors expressed herein do not necessarily state or reflect those of the United States government or Lawrence Livermore National Security, LLC, and shall not be used for advertising or product endorsement purposes. This work performed under the auspices of the U.S. Department of Energy by Lawrence Livermore National Laboratory under Contract DE-AC52-07NA27344.

### **Table of Contents**

1	Introduction.....	6
1.1	Lawrence Livermore National Laboratory (LLNL).....	7
1.2	Commissariat à l'Energie Atomique et aux énergies alternatives (CEA).....	7
2	Event, scenario, and locations.....	8
3	Models description .....	9
3.1	LLNL models .....	9
3.1.1	AEOLUS computational fluid dynamics code.....	9
3.1.2	Lagrangian Operational Dispersion Integrator (LODI) .....	10
3.2	CEA models.....	11
3.2.1	Parallel-SWIFT or PSWIFT .....	11
3.2.2	Parallel-SPRAY or PSPRAY .....	12
3.3	Weather Research Forecast (WRF) model.....	12
4	Computational conditions.....	13
4.1	Source term .....	13
4.1.1	RDD urban source .....	13
4.1.2	Regional scale release .....	14
4.2	Meteorological data .....	14
4.2.1	Raw meteorology: Chicago.....	14
4.2.2	Raw meteorology: Paris .....	15
4.2.3	Processed meteorology inputs: Chicago and Paris .....	15
4.2.4	WRF meteorology forecast.....	16
4.3	Buildings data.....	17
4.4	Simulation matrix .....	18
5	Computational resources and characteristics (mesh, runtime).....	19
5.1	LLNL urban.....	19
5.2	CEA urban .....	20
5.3	Regional modeling: CEA and LLNL .....	21
6	Computational results at local urban scale: Chicago .....	22
6.1	Chicago wind field (wind vector and velocity) .....	22
6.1.1	LLNL results .....	22
6.1.2	CEA results.....	23
6.2	Chicago dispersion (volumetric activity concentration of <sup>137</sup> Cs in air).....	23
6.2.1	LLNL results .....	23
6.2.2	CEA results.....	28
6.3	Chicago radiological exposure (CEA only) .....	31
7	Computational results at local urban scale: Paris.....	33
7.1	Paris wind field (wind vector and velocity).....	33
7.1.1	LLNL results .....	33

7.1.2	CEA results.....	34
7.2	Paris dispersion (volumetric activity concentration of <sup>137</sup> Cs in air).....	35
7.2.1	LLNL results .....	35
7.2.2	CEA results.....	39
7.3	Paris exposure (CEA only) .....	42
8	Computational results at regional scale using the rawinsondes .....	43
8.1	Dispersion (volumetric activity air concentration of Cs-137) .....	43
8.1.1	LLNL results .....	43
8.1.2	CEA results.....	44
8.2	Radiological exposure assessment (Total Effective Dose Equivalent) .....	45
8.2.1	LLNL results .....	45
8.2.2	CEA Results.....	46
9	Computational results at regional scale using WRF wind field.....	47
9.1	Dispersion (volumetric activity air concentration of Cs-137) .....	47
9.1.1	LLNL results .....	47
9.1.2	CEA results.....	49
9.2	Radiological exposure assessment (Total Effective Dose Equivalent) .....	52
9.2.1	LLNL Results .....	52
9.2.2	CEA Results.....	53
10	Modeling Discussion.....	55
10.1	Urban dispersion modeling: LLNL's Aeolus and CEA's PMSS.....	55
10.2	Regional dispersion modeling .....	56
11	Technical Conclusions: model similarities and discrepancies.....	57
12	Table Top Exercise Conclusions .....	58
12.1	Lessons learned from the exercise .....	58
12.2	Possible model improvements .....	60
12.3	Concluding comments on modeling urban releases.....	61
13	Acronyms, definitions, and abbreviations.....	63
14	Acknowledgements.....	64
15	References .....	65
16	Circulation of the report.....	67
17	Appendix A: Details on Aeolus model .....	68
17.1	Turbulence closure .....	68
17.2	Dispersion model.....	68
18	Appendix B: Details on PMSS model.....	70
18.1	Turbulence closure in PSWIFT .....	70
18.2	Dispersion modeling in PSPRAY .....	72
19	Appendix C: Radiological exposure assessment – CEA Method .....	74
20	Appendix D: Radiological exposure assessment – LLNL/NARAC Method.....	76

## 1 Introduction

Atmospheric dispersion modeling is used by public safety personnel for response and emergency planning for potentially damaging releases into the atmosphere. In particular, models are used to determine the consequences of accidental or deliberate releases of nuclear or toxic materials. Many countries maintain national response capabilities to address domestic or international incidents. Collaboration between such organizations has a variety of benefits. In addition to fostering relationships between different disaster response organizations, the joint exercise of such capabilities presents an opportunity to assess the different strengths of distinct technical approaches to dispersion modeling. This can highlight future opportunities for joint model development to the benefit of both parties. In the interest of promoting such an exchange of technical expertise, the US Department of Energy's (DOE) Office of Emergency Operations<sup>3</sup> and the French Commissariat à l'Énergie Atomique et aux énergies alternatives (CEA) requested that Lawrence Livermore National Laboratory's (LLNL) National Atmospheric Release Advisory Center (NARAC) in California host a joint table top exercise with experts in emergency management and atmospheric transport modeling. CEA and LLNL provide emergency response capabilities for their respective nations, as well as engaging in applied research in atmospheric release modeling. This exercise involved a technical exchange between these organizations and comparison of their distinct modeling and response approaches resulting in this joint report. In addition to the interaction between both organizations, the exercise also involved the use of multiple LLNL and CEA models using different levels of sophistication and types of modeling input. Specifically, the urban release simulations used the Parallel-Micro-SWIFT-SPRAY modeling suite embedded in CERES® CBRN-E decision-support system developed at CEA and two versions of the developmental urban release code, Aeolus, developed at LLNL: one optimized for rapid assessment and the other including more realistic physics. Regional scale simulations were carried out with the CEA Parallel-SPRAY (PSPRAY) Lagrangian dispersion model and the LLNL/NARAC operational code, LODI, but using two distinct input types: one used a single meteorological observation while the other leveraged four day WRF forecasts for 3-D wind fields. This exercise was distinct in character from standard exercises carried out by NARAC in that it involved the use of developmental capabilities that would not currently be used in the course of an emergency response scenario. These capabilities serve as a preview of the next generation of CEA and LLNL capabilities that are expected to come online over the next several years, and illustrate the advantages these capabilities will represent over current operational capabilities.

---

<sup>3</sup> The exercise was organized under the auspices of DOE NA-46 Office of International Emergency Management and Cooperation.

## 1.1 Lawrence Livermore National Laboratory (LLNL)

LLNL is a U.S. Department of Energy nuclear security laboratory<sup>4</sup> founded in 1952 and located Livermore, California. A hallmark of LLNL is its ability to deploy multidisciplinary teams rapidly to address critical problems in applied research. NARAC is a United States government funded response capability for atmospheric nuclear releases housed at LLNL. The precursor to the center, ARAC, was established at Livermore in 1973 to integrate current meteorological data, weather forecasts, atmospheric transport models, and dose response information to generate an integrated modeling capability to inform decision makers in the event of a nuclear accident. ARAC and NARAC have provided a real time response capability during the Three Mile Island (1979), Chernobyl (1986), and Fukushima (2011) nuclear disasters. NARAC can also provide predictive modeling support during natural disasters such as fires and volcanic eruptions. Through the International Exchange Program (IXP), a subset of NARAC's capabilities is made available to the IAEA and member country governments. In addition to maintaining a 24-hour disaster response capability, LLNL's NARAC also carries out state-of-the-art research in atmospheric modeling in general and dispersion modeling in particular leveraging other capabilities developed at LLNL.

## 1.2 Commissariat à l'Energie Atomique et aux énergies alternatives (CEA)

The CEA is the French Alternative Energies and Atomic Energy Commission (Commissariat à l'Energie Atomique et aux énergies alternatives), a public body established in October 1945 and a major contributor in research, development and innovation. The CEA mission statement has two main objectives: to become a leading technological research organization in Europe and to ensure that France's nuclear deterrent remains effective in the future. The CEA is active in four main areas: low-carbon energies, defense and global security, information technologies and health technologies. In each of these fields, the CEA maintains a cross-disciplinary culture of engineers and scientists, building on the synergies between fundamental and applied research. The CEA has ten research centers in France, each specializing in specific fields. The laboratories are located in the vicinity of Paris and in six French regions where the CEA benefits from the partnerships forged with other research centers, local authorities and universities.

In the field of Atmospheric Transport & Dispersion (AT&D), the CEA has developed modeling capabilities applied to both safety requirements, which the CEA must satisfy as the operator of nuclear facilities (e.g. research reactors, laboratories, and factories), and defense and security programs (verification of the compliance with the CTBT, response to nuclear or non-nuclear proliferation, and CBRN-E threats). Modeling and decision-support systems integrate weather prediction and AT&D chained with health and environmental impact assessment modules.

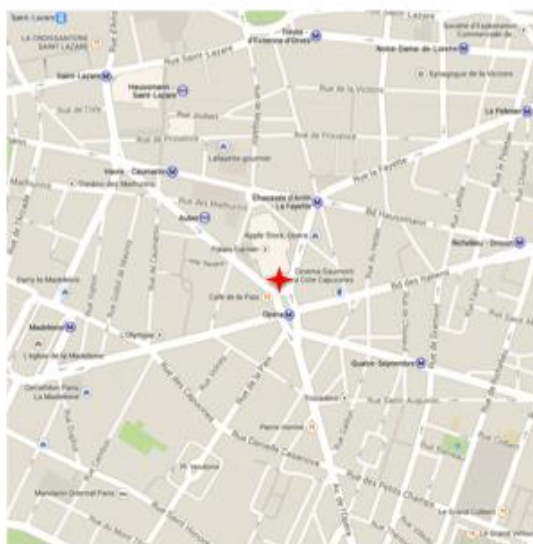
---

<sup>4</sup> The two other National Nuclear Security Administration's laboratories are Los Alamos and Sandia National Laboratories.

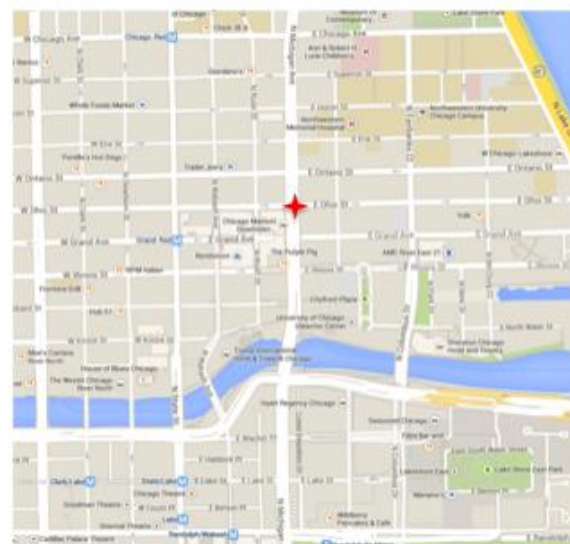
Simulations are carried out routinely at all spatial and temporal scales, from global to meso- and local scales on adaptable computational resources including massively parallel HPC. Results support fundamental research, planning studies, and operational real-time response. In support of this mission, the CEA has a 24/7 modeling capability for accidents that could affect its centers and facilities.

## 2 Event, scenario, and locations

Credible atmospheric release scenarios include nuclear facility accidents and radiological dispersal device (RDD) release. A set of well-defined, shared scenarios was required to exercise and assess the respective LLNL/NARAC and CEA modeling approaches. The primary chosen scenario was a large radiological dispersal device (RDD) release in an urban area. To explore modeling sensitivity, two cities (Paris and Chicago) were chosen as well as two release times (early summer day and night) for each city. This provided two extreme variants of urban skylines and street networks along with some variability in atmospheric behavior for model comparison. The urban setting was selected both due to the interest in exercising a disaster response capability and because the modeling of releases in urban settings is known to be complicated by building effects, such as street channeling and convergence / divergence zones, an area of active research in the atmospheric modeling community.



Paris Release – Palais Garnier



Chicago Release – E. Ohio and N. Michigan

**Figure 1 Release locations for urban dispersion simulations; Paris (left) has relatively uniform building heights and a complex street network, while Chicago (right) has a skyline of variable building heights along a gridded street network.**

The Paris release location was directly to the south of the Palais Garnier on rue Scribe, while the Chicago location was at the intersection of East Ohio Street and North Michigan Avenue. Figure 1 shows the source locations, both located in the heart of their respective cities. Distinct features of each city are anticipated to influence dispersal. Notably, (1) Paris exhibits more consistent lower building heights than does Chicago; (2) Chicago has a more regular gridded street layout than Paris; and, (3) unlike Paris, Chicago is located off a large body of water that affects wind flow.

The hypothetical RDD for all urban scenarios was a 5,000 Ci Cs-137 source with geometric properties consistent with a moderate explosion. Release details were selected not to be representative of any particular potential or historical scenario, but simply to demonstrate the use of the urban models. A release of such magnitude generates a city-block scale plume trackable over an extended period of time; the limited lofting ensures that most material remains close to the ground where it is subject to flow complexity induced by buildings.

In addition to modeling urban releases at high resolution, larger scale regional simulations were also carried out to exercise additional capabilities and evaluate the effects of different meteorological models on larger scales. A much larger hypothetical radiological release of 500,000 Ci Cs-137 over six hours was used for the regional simulations since smaller RDD-like releases are not significant at such large scales.

### 3 Models description

#### 3.1 LLNL models

##### 3.1.1 *AEOLUS computational fluid dynamics code*

Aeolus is an efficient three-dimensional (3D) computational fluid dynamics (CFD) code based on a finite volume method developed for predicting transport and dispersion of contaminants in a complex urban area. It solves the time dependent incompressible Navier-Stokes equations on a regular Cartesian staggered grid using a fractional step method. It also solves a scalar transport equation for temperature that is incorporated using a Boussinesq approximation. The model includes a Lagrangian dispersion model for predicting transport and dispersion. The model can be run in a very efficient RANS (Reynolds Average Navier-Stokes) mode or a higher resolution but computationally demanding LES (Large Eddy Simulation) mode (see the Appendix A).

In RANS mode, the model produces a steady state solution for the 3D velocity field. The wind is based on the 3D RANS equations for incompressible flow using a zero equation (algebraic) turbulence model based on Prandtl's mixing length theory (Gowardhan, et al., 2011). The selection of the zero-equation turbulence model was made so as to reduce the run time of the

CFD simulation, thereby making it more closely adapted for a fast-response application (Chen & Xu, 1998). More complex turbulence models could also be considered. However, given that there has been no evidence of clear superiority or unique suitability of one model over the others for all wind flow applications in real urban geometries, using a zero-equation model was considered acceptable in the context of this exercise. The governing RANS equations are solved explicitly in time until steady state is reached using a projection method. At each time step of the projection method, the divergence-free condition is not strictly satisfied to machine precision levels, but rather when steady state is reached incompressibility is recovered. This makes the method comparable to the artificial compressibility method (Chorin, 1968). The RANS equations are solved on a staggered mesh using a finite volume discretization scheme that is second-order accurate in space (central difference) and time (Adams–Bashforth). The law-of-the-wall was imposed at all of the solid surfaces. The pressure Poisson equation was solved using the successive over-relaxation (SOR) method. A free slip condition was imposed at the top boundary and the side boundaries, while an outflow boundary condition is used at the outlet.

Aeolus also includes a high fidelity LES mode (Neophytou, et al., 2011). Large eddy simulation resolves larger turbulent motions of the flow field solution allowing better fidelity than alternative approaches such as RANS methods. It also models the smallest scales of the solution, rather than resolving them as direct numerical simulation (DNS) does. This makes the computational cost for practical engineering systems with complex geometry or flow configurations attainable using supercomputers. In contrast, direct numerical simulation, which resolves every scale of the solution, is prohibitively expensive for nearly all systems with complex geometry or flow configurations. Details on Aeolus' handling of turbulence closure and dispersion modeling can be found in Appendix A of this report.

### *3.1.2 Lagrangian Operational Dispersion Integrator (LODI)*

LODI is a regional atmospheric Lagrangian particle dispersion model (LPDM) developed for operational emergency response at LLNL's NARAC. It solves the 3D advection diffusion equation using a Lagrangian Monte Carlo method that calculates possible trajectories of fluid "particles" in a turbulent flow. Particles are marked at the source of a contaminant with an appropriate amount of contaminant mass based upon prescribed mass emission rates. These computational particles can also be given a total density and diameters sampled from input aerosol size distribution, which are used to calculate gravitational settling and deposition. Initial particle positions are assigned by sampling the spatial distribution based on the geometry of the source. A large number of independent particle trajectories are calculated by moving particles in response to the various processes, such as mean wind advection, gravitational settling, and turbulent mixing, represented within the simulation. The mean contaminant air concentration is estimated from the spatial distribution of the particles at a particular time.

Wind fields can be derived diagnostically from observational meteorological data or from a prognostic forecast model, such as the Weather Research Forecast (WRF) model discussed below. Turbulent dispersion is modeled via a random walk process with atmospheric eddy diffusivity values to parameterize unresolved turbulent motions. Radioactive decay and production as well as wet and dry deposition can be simulated. The features of this model are described in greater detail in Leone *et al.* (2001).

## 3.2 CEA models

CERES® CBRN-E is a flexible modeling and decision-support system designed for dispersion simulation and impact assessment of accidental or deliberate atmospheric releases of hazardous material. CERES® includes three dispersion models: standard Gaussian and urbanized Gaussian models in its operational version, and LPDM in a development version dedicated to research. The LPDM model is based on the Parallel-Micro-SWIFT-SPRAY (PMSS) modelling system. PMSS (Duchenne, et al., 2011) (Oldrini, et al., 2011) includes parallelized models PSWIFT and PSPRAY.

### 3.2.1 Parallel-SWIFT or PSWIFT

PSWIFT is an analytically modified mass consistent interpolator over complex terrain and urban areas. Given topography, meteorological data and building geometry, a mass consistent 3D wind field is generated. PSWIFT is also able to derive diagnostic turbulence parameters (namely, the turbulent kinetic energy, and its dissipation rate) to be used by PSPRAY especially inside the flow zones modified by obstacles. Details on PSWIFT handling of turbulence closure can be found in Appendix B of this report.

Input data can be on-site measurements, user-defined data to study a specific scenario, or forecast predictions from a larger-scale meteorological model. Depending on the meteorological data, several interpolation procedures are available that give a first estimate for flow boundary conditions, particularly at the lateral boundary and domain top. If obstacles such as buildings are included in a local scale simulation, their influence is modeled using a Röckle type prescription on the flow structure. The influence of atmospheric stability on the wind flow over terrain is modeled using a weighting factor  $\alpha$ , which is the ratio of the horizontal wind component to the vertical wind component.

The adjustment to terrain and obstacles ensures mass conservation of the wind field by forcing realistic boundary conditions (zero flux at ground and domain top levels) and adjusting both horizontal and vertical velocity components. The following two criteria are taken into account:

- Mass conservation for an incompressible fluid with constant  $\rho$  i.e.  $\text{div}\vec{V} = 0$ ;

- Constraint to be as close as possible to the initial interpolated wind field.

A functional is then defined in which the incompressibility constraint is introduced through a Lagrangian multiplier  $\lambda$  and is minimized using a Gauss-Seidel SOR procedure.

### 3.2.2 *Parallel-SPRAY or PSPRAY*

PSPRAY is a LPDM able to account for the presence of obstacles. It is directly derived from the SPRAY code (Tinarelli, et al., 2007) (Tinarelli, et al., 2013) and it is based on a 3D form of the Langevin equation for the random velocity (Thomson, 1987).

The velocity of the particles is mainly characterized by two components: a mean component, or “transport-component”, which is defined by the mean velocity of the local wind, and a stochastic component, which simulates dispersion and reproduces the atmospheric turbulence. Mean values for wind-speed are computed by PSWIFT and provided to PSPRAY as a model input. The stochastic fluctuation term is the solution of a system of differential stochastic equations reproducing the statistical features of local atmospheric turbulence. In the Thomson (1987) model, different options are proposed in order to solve the involved equations, such as schemes based on the probability density function of turbulent bi-Gaussian velocities with different closures or Gram-Charlier series expansions. Details on PSPRAY modeling of the numerical particles trajectories can be found in Appendix B of this report.

When PSPRAY is run with obstacles, the model also treats bouncing against obstacles. According to the obstacles structure provided by PSWIFT, particles crossing the intersection between a free and a full cell are subjected to an elastic impact and rebound.

Moreover, PSPRAY is also able to compute the dry and wet deposition of the numerical particles on all accessible (exposed) surfaces: not only ground, but also walls, roofs and ceilings. It can evaluate the infiltration in the buildings as the “exfiltration” out of them using a 3D external pressure field and characteristic times for venting.

## 3.3 Weather Research Forecast (WRF) model

The numerical weather prediction (NWP) model used to generate time varying, three-dimensional wind fields for this exercise was the non-hydrostatic, fully compressible Weather Research and Forecast (WRF) model (Skamarock, et al., 2008). Specifically, version 3.5.1 of the advanced research dynamical core of the WRF code was used. WRF is a flexible community-based atmospheric model designed to address both operational weather forecasting and broad atmospheric research needs. WRF was developed via collaboration among numerous academic, research, and government organizations to streamline the transfer of atmospheric research

findings to an operational capacity. The large set of available model physics schemes and data assimilation approaches coupled with efficient model nesting make WRF appropriate for performing simulations on scales of motion from tens of meters to thousands of kilometers. Source code for WRF is available for download by the public at no cost through a National Center for Atmospheric Research (NCAR) supported website<sup>5</sup>.

## 4 Computational conditions

### 4.1 Source term

#### 4.1.1 RDD urban source

As discussed above in Section 2, the urban scenarios were a prompt hypothetical RDD release of 5,000 Ci (60 grams of Cesium-137) resulting in a city-block scale plume remaining close enough to the ground. Neither the LLNL nor CEA urban release models include explicit modeling of explosive releases, so simplified geometric representations were used. Slightly different source term assumptions were made for each. The NARAC source term was treated as sphere of 5-meter radius ascending at a rate of 1 m/s for 60 seconds. The particle size was modeled as a truncated log-normal distribution with a median of 1 micron, a unitless geometric standard deviation of 3, and range between 0.1 and 10 microns. The corresponding CEA source term was a cylinder with a radius of 5 meters and a height of 65 meters, and all particles were treated as having a size of 1 micron. Figure 2 illustrates the differences.

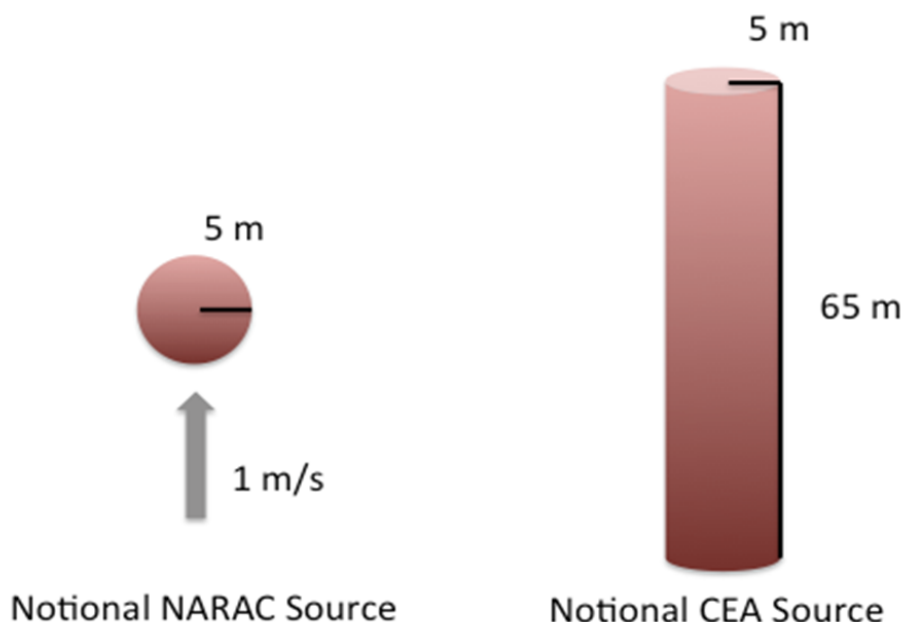


**Figure 2** Illustration of source term models for NARAC and CEA urban release simulations. NARAC: a lofting source with a log-normal particle size distribution; CEA: a cylindrical source with a mono-disperse aerosol.

<sup>5</sup> [http://www2.mmm.ucar.edu/wrf/users/download/get\\_source.html](http://www2.mmm.ucar.edu/wrf/users/download/get_source.html)

#### 4.1.2 Regional scale release

A much larger hypothetical radiological release of 500,000 Ci (6 kg of Cs-137) over six hours was used for the regional simulations since smaller RDD-like releases are not significant at such large scales. The LLNL model used the same particle size distribution as in the urban case; however the 5-meter radius spherical source was held at a constant 5-meter height. The CEA model used a cylindrical source with a radius of 5 meters and a height of 5 meters, and all particles were treated as having a size of 1 micron.

## 4.2 Meteorological data

Two kinds of meteorological data were used in the course of the exercise. The first took data from a single “canned” meteorological observation and assumed that wind direction was constant and wind speed varied only with height. This was the only type of data used for the high-resolution urban models. For the regional models, the single vertically-varying profile was used as one of the meteorology inputs, and a second high resolution predictive forecast made using time-varying WRF wind fields.

### 4.2.1 Raw meteorology: Chicago

The Chicago day and night meteorology was based on observations from 1 June 2014 at 00:00 UTC and 27 May 2014 at 12:00 UTC, respectively. These data were used for both urban and regional simulations. The direction and speed as a function of height are tabulated in Table 1 and Table 2 for day and night, respectively.

**Table 1 Raw meteorology for Chicago day, 1 June 2014 at 00:00 UTC.**

Height (m)	Wind speed (m/s)	Wind Direction (degrees)
10	5.1	175
380	5.7	160
589	6.2	165
685	5.7	165
990	7.7	165
1321	8.2	160

**Table 2 Raw meteorology for Chicago night, 27 May 2014 at 12:00 UTC.**

Height (m)	Wind speed (m/s)	Wind Direction (degrees)
10	2.1	270
380	10.3	275
556	11.3	280
685	11.3	280
990	9.8	265
1281	9.8	265

#### 4.2.2 Raw meteorology: Paris

The Paris day and night meteorology was based on observations from 5 June 2014 at 12:00 UTC and 13 May 2014 at 00:00 UTC, respectively. These data were used for both urban and regional simulations. The direction and speed as a function of height are tabulated in Table 1 and Table 2 for day and night, respectively.

**Table 3 Raw meteorology for Paris day, 5 June 2014 at 12:00 UTC.**

Height (m)	Wind speed (m/s)	Wind Direction (degrees)
10	3.6	230
604	5.1	235
1295	6.7	245

**Table 4 Raw meteorology for Paris night, 13 May 2014 at 00:00 UTC.**

Height (m)	Wind speed (m/s)	Wind Direction (degrees)
10	2.1	230
612	11.3	290
1295	10.8	290

#### 4.2.3 Processed meteorology inputs: Chicago and Paris

The single observations for each location and time were used to generate the vertical wind profiles shown in Table 5 used as input for both urban and regional simulations. Due to the relatively low height of the urban simulation domain, only the wind direction from the ground level observation is used.

**Table 5 Processed meteorology input for Chicago and Paris, both day and night.**

	Wind speed profile $\left\{ u = \frac{u_{ref}}{\ln\left(\frac{z_{ref}}{z_0}\right)} \ln\left(\frac{z}{z_0}\right) \right\}$			Inflow profile (see Figure 3)	Wind Direction (Constant with height)
	$u_{ref}$ (m/s)	$z_{ref}$ (m)	$z_0$ (m)		
<b>Chicago (Day)</b>	5.7	380	0.0001	Figure 3A	175°
<b>Chicago (Night)</b>	10.3	380	2.0	Figure 3B	270°
<b>Paris (Day)</b>	5.1	604	0.001	Figure 3C	230°
<b>Paris (Night)</b>	11.3	612	2.0	Figure 3D	230°

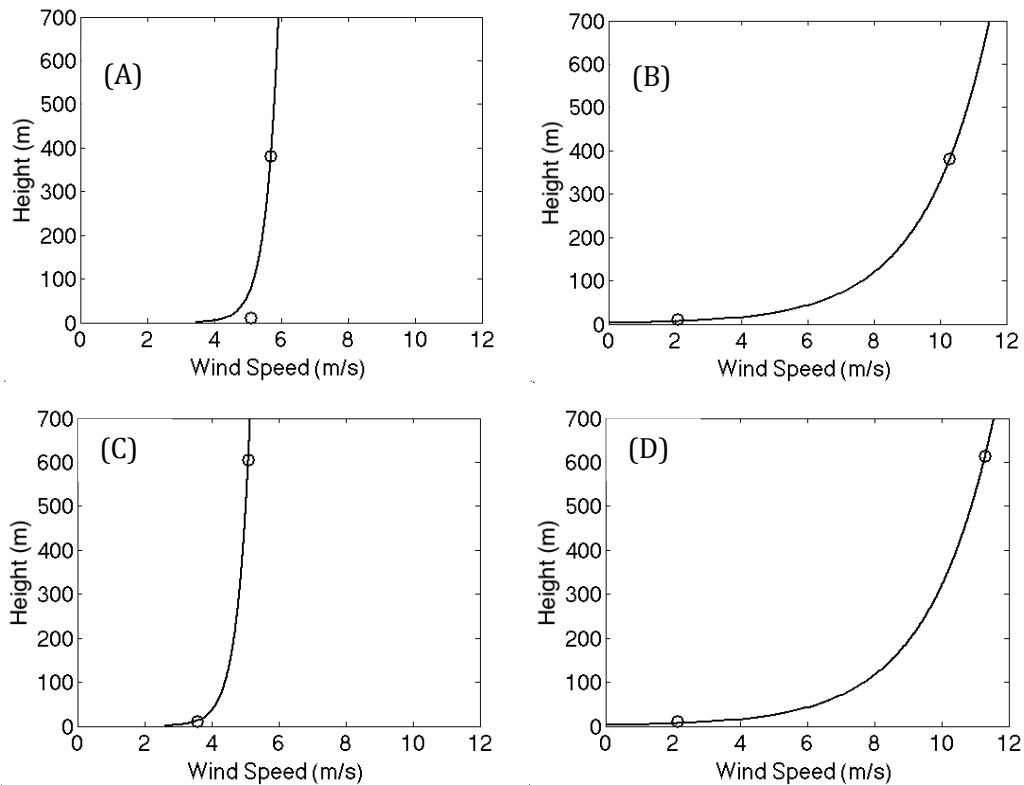


**Figure 3** Inflow profiles for (A) Chicago day, (B) Chicago night, (C) Paris day, and (D) Paris night.

#### 4.2.4 WRF meteorology forecast

Higher resolution three-dimensional WRF simulations were used for a subset of the regional simulations. Initial and lateral boundary conditions for the WRF forecasts were provided by the Global Forecast System (GFS). The GFS gridded data fields were available at half-degree resolution at three-hour intervals. In addition, metar, maritime, and mesonet data platform weather observations from the Meteorological Assimilation Data Ingest System (MADIS) (Miller, et al. 2005, Miller et al. 2009) were used for a 6-hour model initialization spin up. A snapshot of the start of the high resolution WRF run used for the Chicago day run is illustrated in Figure 4. Note that an on shore lake breeze develops due to land and water temperature discrepancies typical for Chicago during the daytime. The final WRF simulation covered a 96-hour period starting on 17 June 2014. This date is different from those used for the canned meteorology based simulations, so direct comparison of, for example, wind direction would not be productive.

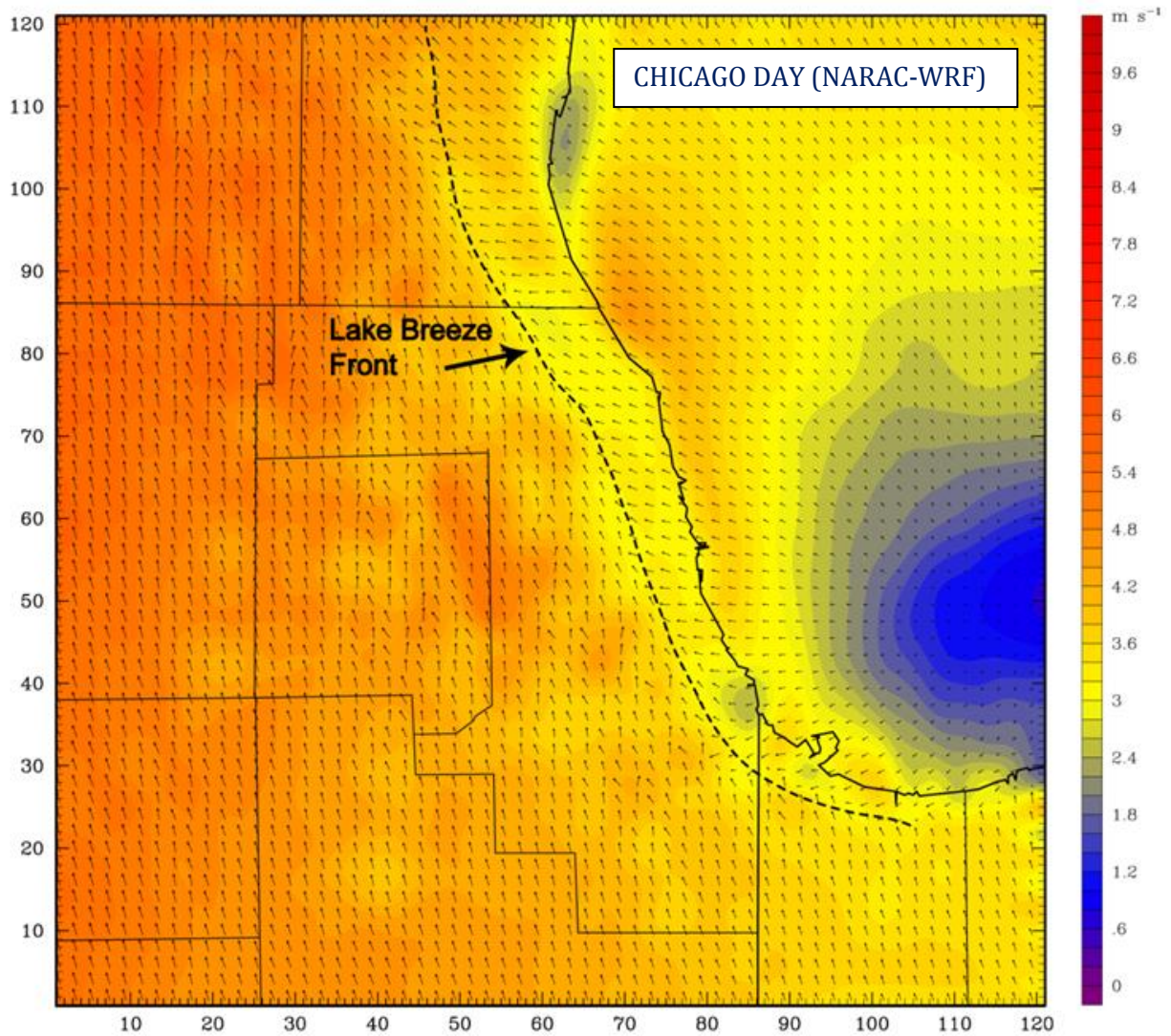


Figure 4 Snapshot of notional high resolution WRF run for the Chicago region. The vectors and wind speed are in m/s and the front created by the on shore breeze of Lake Michigan is illustrated.

### 4.3 Buildings data

Shapefiles were used to build the urban grid for the two cities (Figure 5). The Chicago shapefile was downloaded from the City of Chicago official website<sup>6</sup>. The Paris shape file is part of the BD TOPO® database, produced by the French National Geographic Institute (IGN)<sup>7</sup>.

<sup>6</sup> [http://www.cityofchicago.org/city/en/depts/doi/supp\\_info/gis\\_data.html](http://www.cityofchicago.org/city/en/depts/doi/supp_info/gis_data.html)

<sup>7</sup> <http://professionnels.ign.fr/bdtopo>

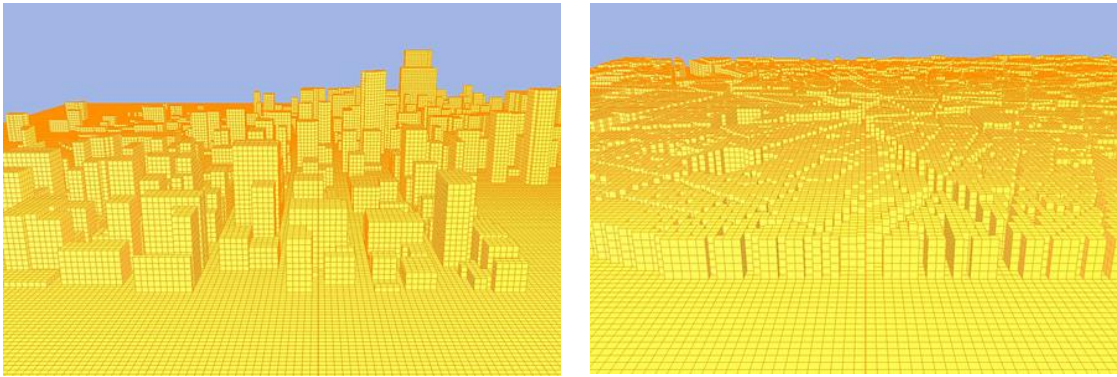


Figure 5 Computational grids for Chicago (left) and Paris (right) built using acquired shapefiles.

#### 4.4 Simulation matrix

The complete set of simulations performed for the TTX by LLNL and CEA are listed in Table 6. This table also includes a high level summary of the source conditions and the type of meteorology employed. Table 7 lists the start and stop time for each different type of simulation, i.e., for urban and regional, for day and night, and for Paris and Chicago.

Table 6 Simulation matrix for Chicago and Paris, both day and night.

Description	Source strength	Source type and duration	Meteorology	Chicago Day	Chicago Night	Paris Day	Paris Night
Urban Diagnostic (CEA)	5e3 Ci Cs-137	Instantaneous column	Table 5	X	X	X	X
Urban RANS (LLNL)	5e3 Ci Cs-137	Figure 2, rising sphere	Table 5	X	X	X	X
Urban LES (LLNL)	5e3 Ci Cs-137	Figure 2, rising sphere	Table 5		X		X
Regional (CEA, LLNL)	5e5 Ci Cs-137	Point, six hours	Table 5	X	X		
Regional (CEA, LLNL)	5e5 Ci Cs-137	Point, six hours	WRF	X	X	X	X

Table 7 Simulation start and stop time (all in UTC).

Description	Chicago start	Chicago stop	Paris start	Paris stop
Urban day	00:00 1 June	00:30 1 June	12:00 5 June	12:30 5 June
Urban night	12:00 27 May	12:30 27 May	00:00 13 May	00:30 13 May
Regional day	00:00 1 June	00:00 5 June	n/a	n/a
Regional night	12:00 27 May	12:00 31 May	n/a	n/a
Regional day, WRF	19:00 17 June	19:00 21 June	09:00 17 June	09:00 21 June
Regional night, WRF	06:00 17 June	06:00 21 June	01:00 17 June	01:00 21 June

## 5 Computational resources and characteristics (mesh, runtime)

### 5.1 LLNL urban

Aeolus uses a second order accurate central difference and QUICK scheme for advective terms and second order accurate central difference for diffusive terms. The temporal integration is done using Adams-Bashforth scheme, which is also second order accurate. The pressure Poisson equation is solved efficiently using multigrid technique.

Figure 5 shows the computational grids built from the building shapefiles as employed for Aeolus simulations. Mesh resolution was 5 meters in all directions. Aeolus uses a matrix encoding of 0 for fluid cells and 1 for solid cells to efficiently handle building effects. Full mesh details are given in Table 8.

**Table 8** Details of LLNL Aeolus computational grid.

	$L_x$	$L_y$	$L_z$	$dx$	$dy$	$dz$	Grid Points
Chicago	2.8 km	2.82 km	0.4 km	5 m	5 m	5 m	25.5 Million
Paris	2.6 km	2.35 km	0.4 km	5 m	5 m	5 m	20.0 Million

Both RANS and LES versions of AEOLUS were run on a MacPro desktop workstation. RANS simulations required on the order of 5 minutes to complete, while LES simulations required on the order of 5 hours. A complete summary of processor utilization and run time is given in Table 9.

**Table 9** LLNL urban simulation details.

	Wind simulation duration	# Processor	Run time	Particle simulation duration	# Particles	# Processor	Run time
<b>Chicago (Day) RANS</b>	1800 sec	8	6 min	1800 sec	600 000	1	5 min
<b>Chicago (Night) RANS</b>	1800 sec	8	6 min	1800 sec	600 000	1	5 min
<b>Paris (Day) RANS</b>	1800 sec	8	4 min	1800 sec	600 000	1	4 min
<b>Paris (Night) RANS</b>	1800 sec	8	4 min	1800 sec	600 000	1	4 min
<b>Chicago (Night) LES</b>	1800 sec	8	-	1800 sec	600 000	8	6 hrs
<b>Paris (Night) LES</b>	1800 sec	8	-	1800 sec	600 000	8	5 hrs

## 5.2 CEA urban

Computations were performed using one node of the massive parallel computer called “airain”, which is located at the Research and Technology Computing Center (CCRT – Centre de Calcul Recherche et la Technologie). One node contains 2 ten-core CPU Ivy Bridge processors clocked at 2.8 GHz and has 64 GB of memory.

For both Chicago and Paris cases, computational grids were defined with a horizontal mesh resolution of 3 meters. The vertical grid was regular inside the urban canopy and relaxed above to the top of the domain. The grid defined for the Chicago location had 37 vertical levels from the ground to a height of 1000 meters, with 26 regular levels from the ground to a height of 100 meters. The grid defined for the Paris location had 31 vertical levels from the ground to a height of 800 meters, with 21 regular levels from the ground to a height of 60 meters. Full mesh details are given in Table 10.

**Table 10 Details of CEA computational grid.**

	$L_x$	$L_y$	$L_z$	$dx$	$dy$	$dz$	Grid Points
Chicago	2.7 km	2.7 km	1 km	3 m	3 m	varying with height	30 Million
Paris	2.52 km	2.28 km	0.8 km	3 m	3 m	varying with height	19.8 Million

A complete summary of processor utilization and run time is given in Table 11. Particle simulations include deposition on ground and all accessible surfaces (walls, roofs and ceilings). The same computations without computing deposition were faster (8.5 minutes for Paris case instead of 11 minutes).

**Table 11 CEA urban simulation details**

	Wind simulation duration	# Processor	Run time	Particle simulation duration	# Particles	# Processor	Run time
<b>Chicago (Day)</b>	1800 sec	5	5 min	1800 sec	600 000	8	8.5 min
<b>Chicago (Night)</b>	1800 sec	5	5 min	1800 sec	600 000	8	7.5 min
<b>Paris (Day)</b>	1800 sec	5	6 min	1800 sec	600 000	8	11 min
<b>Paris (Night)</b>	1800 sec	5	6 min	1800 sec	600 000	8	11 min

### 5.3 Regional modeling: CEA and LLNL

A total of three model domains were used for the WRF atmospheric modeling portion of the exercise for both the Chicago and Paris locations. The outermost model domain had a horizontal grid spacing of 9 km and was able to simulate large-scale weather systems as they propagate across the study region. Nested model domain 2 had a horizontal grid spacing of 3 km. The innermost model domain had a horizontal grid spacing of 1 km, which is sufficient to resolve the wind fields and any small-scale atmospheric features present in Chicago and Paris due to the absence of any major complex terrain. A fixed numerical time step of 5 seconds was utilized for the high-resolution inner domain. A total of 50 terrain-following vertical sigma levels were utilized for the WRF simulations. The sigma level distribution was designed to generate a vertical resolution of approximately 15 - 20 m in the lowest 200 m of the atmosphere. The full 96-hour forecast required about 80 minutes to run on 96 cores from a 3.47 GHz Intel Xeon cluster.

LODI (NARAC) regional simulations were run on 24 processors, and required ~1 minute for canned meteorology cases and ~10 minutes for WRF forecast cases. PSPRAY (CEA) regional simulations were run on 12 processors, and required ~6 minute for canned meteorology cases and ~7 minutes for WRF forecast cases.

## 6 Computational results at local urban scale: Chicago

PMSS (mass-consistent diagnostic flow model and Lagrangian Particle Dispersion model) was used by CEA for the day and night Chicago release scenarios. Fast-running (RANS) and high-fidelity (LES) model Aeolus runs were carried out by LLNL/NARAC for the day and night Chicago release scenarios. Since Aeolus is a development code, some of the metrics of interest (e.g. deposition, integrated dose) have not been fully implemented. For this reason, the metrics for direct comparison between simulations were static wind fields and air concentration values over time.

### 6.1 Chicago wind field (wind vector and velocity)

#### 6.1.1 LLNL results

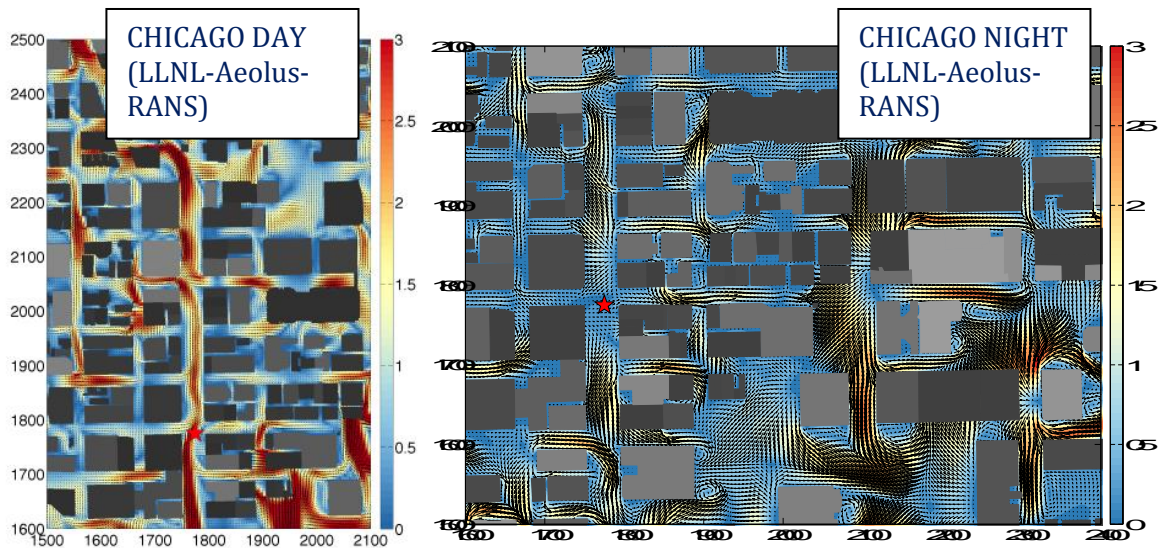


Figure 6 LLNL RANS Wind field for Chicago day (left) and night (right). Grid size is in meters. Wind speed presented in m/s.

Figure 6 shows the time averaged wind speed magnitude and velocity vectors in a horizontal slice at street level for Chicago. For the day case, the inflow winds are from south-south-east (175 degrees) and are not precisely aligned with the streets. In spite of this, channeling effects are produced along both north-south and east-west running streets. For the night case, the winds are from west (270 degrees) and perfectly aligned with the street grid. This causes higher momentum air striking the building faces to be diverted downward and compete with the inflow at the street level, producing divergence zones and recirculation regions. There are also saddle point features, where high velocity fluid is deflected down the surface of tall buildings and out along streets parallel to the face. The presence of these phenomena means that even though the inflow wind speed is higher for the nighttime case, the street level wind speeds are lower due to these turbulent regions. This shows that in highly complex urban areas even slight changes in

wind direction can make huge differences in the wind field. Physics based modeling is required to capture such complex behavior.

### 6.1.2 CEA results

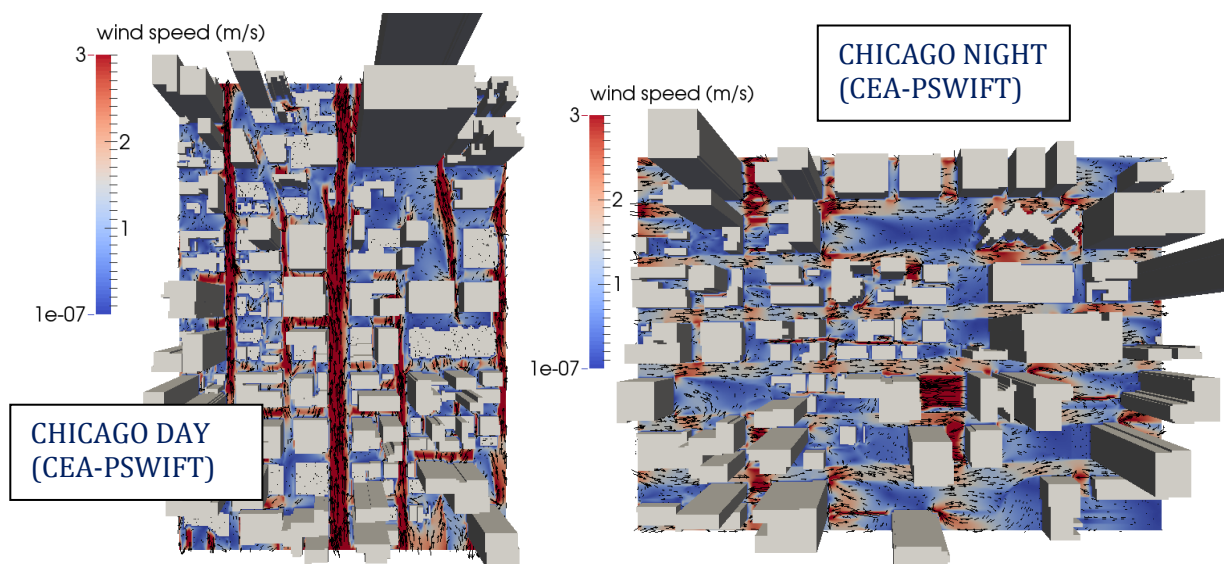


Figure 7 CEA PSWIFT Wind field for Chicago day (left) and night (right). Wind speed presented in m/s.

Figure 7 shows the time averaged wind speed magnitude and velocity vectors in a horizontal slice at three-meter height for Chicago. At this level, inflow wind speed is about 3 m/s for the day case and less than 1 m/s for the night case. For the day case, the inflow winds are quite parallel with streets with a south-north orientation, so that we observe channeling inside these streets. In transverse streets, wind speed is lower and the flow is more complex due to canyon effects. For the night case, the inflow winds are aligned with the streets which are west-east oriented giving a general trend of the air motion from west to east. However, the flow pattern between the buildings is extremely complex with re-circulations and turbulent eddies in both horizontal and vertical planes. These two cases demonstrate that even in a regular urban configuration, flows are essentially 3D and require full (or, at least, simplified) resolution of the effects of urban structures on fluid flow.

## 6.2 Chicago dispersion (volumetric activity concentration of $^{137}\text{Cs}$ in air)

### 6.2.1 LLNL results

Fast-running RANS mode simulations were carried out for both the day and night case in Chicago. Figure 8 shows 1 minute averaged concentration contours in  $\text{Ci}/\text{m}^3$  at street level at different time steps for the daytime case<sup>8</sup>. There is very little upwind dispersion near the source

<sup>8</sup> For every Curie, there are 12 milligrams of Cs-137.

due to the dominance of street channeling in this scenario. Within 10 minutes the plume is around 1,000 meters wide, and particles start to exit the domain (~1,000 m from source) after 20 minutes.

Figure 9 shows 1 minute averaged concentration contours at street level at different time steps for the Chicago night case. In contrast to the day case, the simulation exhibits upwind dispersion near the source due to the presence of divergence zones. The faster wind speed during nighttime should lead to a narrower plume, but due to these divergence zones, the nighttime plume width is similar to the daytime. As in the daytime case, the plume starts to exit the domain (~1,000 m from source) after 20 minutes. In spite of the fact that the nighttime inflow wind speed is almost twice as fast as the daytime wind speed, the divergences regions created at the street level substantially reduce the transport speed of the plume, resulting in similar exit times.

In addition to the fast-running RANS dispersion models, the higher-fidelity large eddy simulation (LES) mode was also applied to the nighttime case for comparison purposes (Figure 10). Each voxel shows instantaneous concentration level (blue-lower concentration and red-higher concentration). Both the downwind and crosswind spread are consistent with the RANS simulation. Figure 11 shows that the divergence zones lead to considerable vertical dispersion in the LES model.

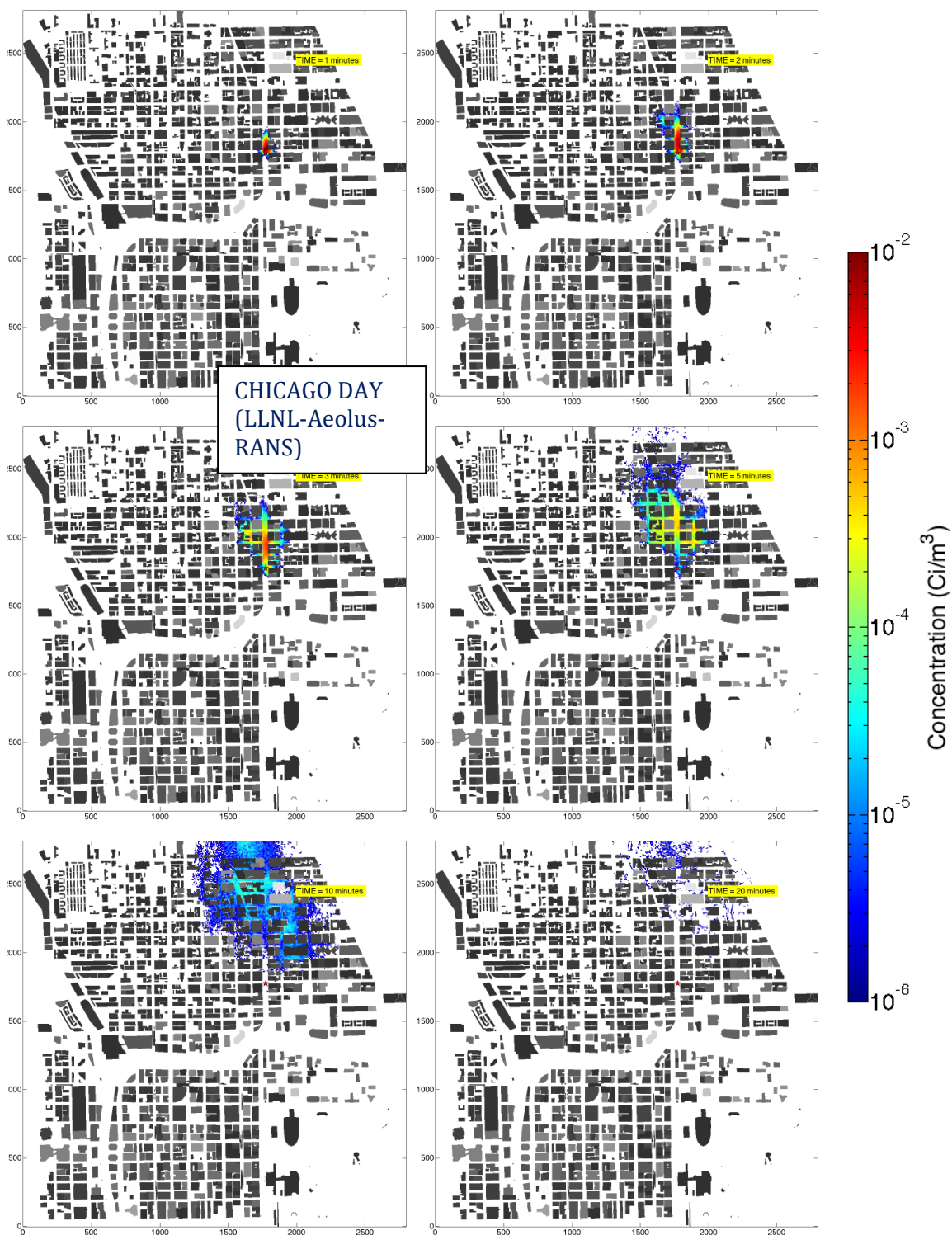


Figure 8 Chicago day RANS air concentration in Ci/m<sup>3</sup> at different time snapshots up to 20 minutes after release (scale is logarithmic; red is 10<sup>-2</sup> Ci/m<sup>3</sup> and deep blue is 10<sup>-6</sup> Ci/m<sup>3</sup>); from left to right, top to bottom, t = 1 minute, 2 minutes, 3 minutes, 5 minutes, 10 minutes, and 20 minutes.

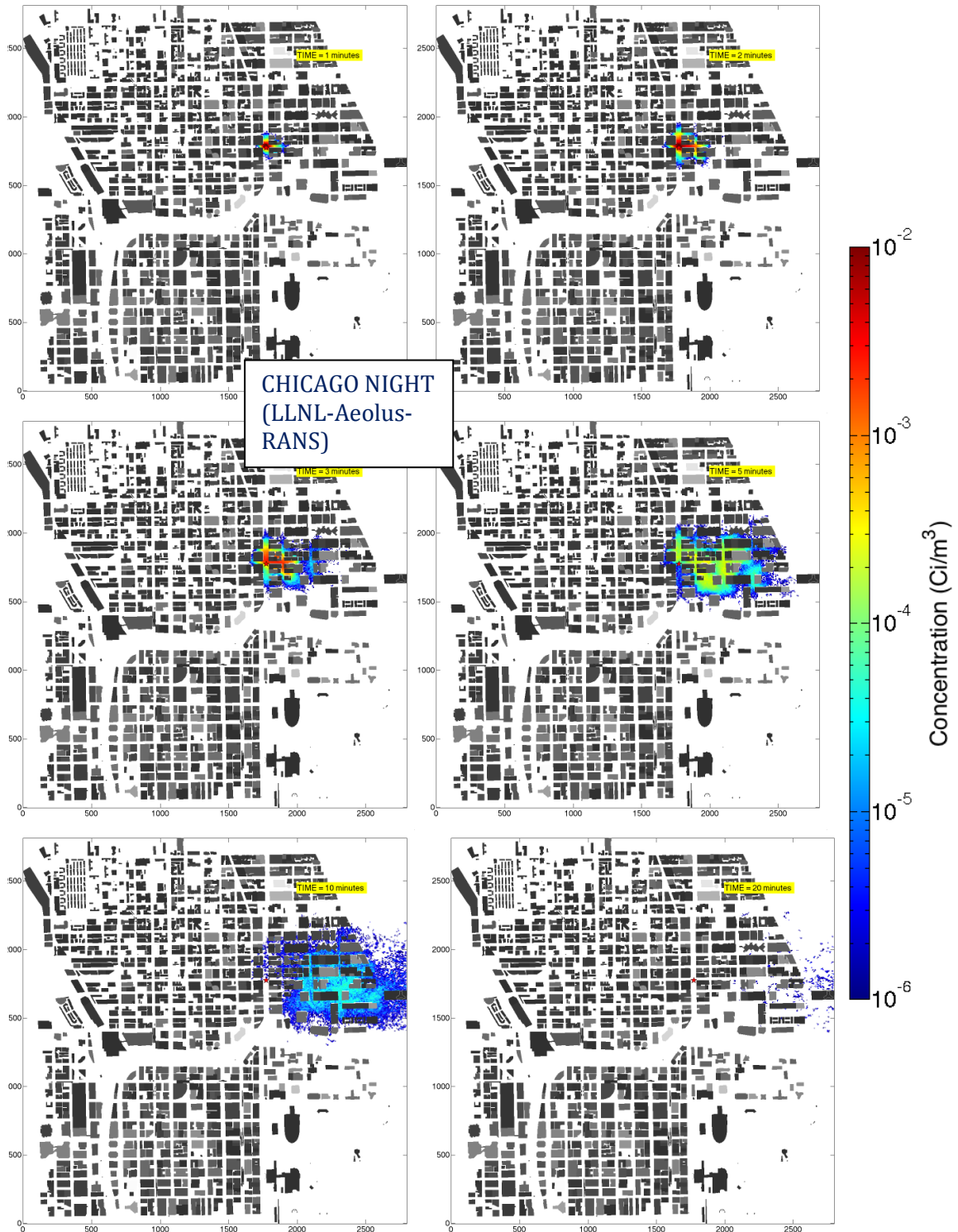


Figure 9 Chicago night RANS air concentration in  $\text{Ci/m}^3$  at different time snapshots up to 20 minutes after release (scale is logarithmic; red is  $10^{-2} \text{ Ci/m}^3$  and deep blue is  $10^{-6} \text{ Ci/m}^3$ ); from left to right, top to bottom,  $t = 1$  minute, 2 minutes, 3 minutes, 5 minutes, 10 minutes, and 20 minutes.

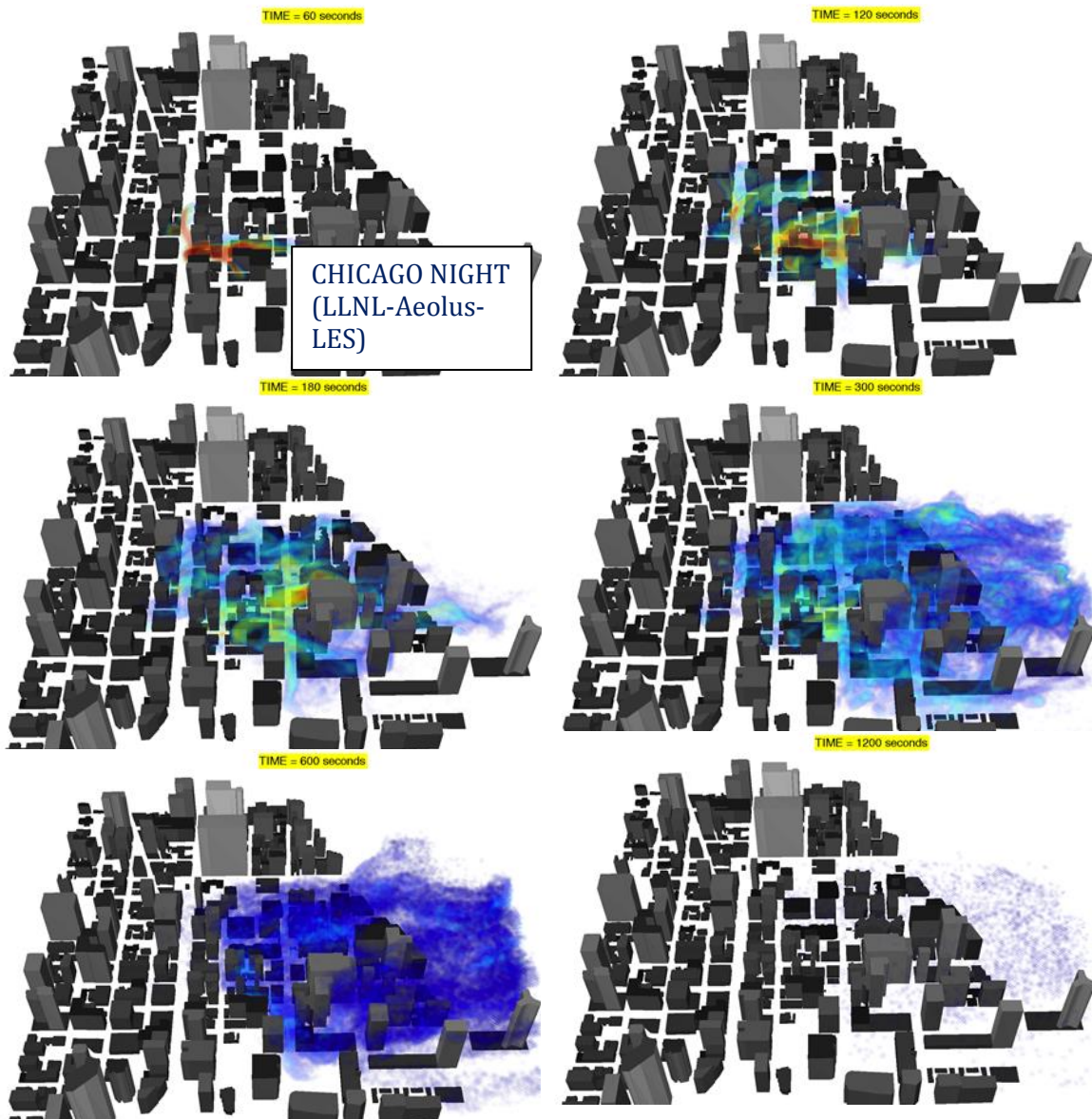


Figure 10 High fidelity LES simulation for Chicago nighttime scenario at different time snapshots up to 20 minutes after release (concentration scale is logarithmic; red is  $10^{-2}$  Ci/m<sup>3</sup> and deep blue is  $10^{-6}$  Ci/m<sup>3</sup>); from left to right, top to bottom,  $t = 1$  minute, 2 minutes, 3 minutes, 5 minutes, 10 minutes, and 20 minutes.

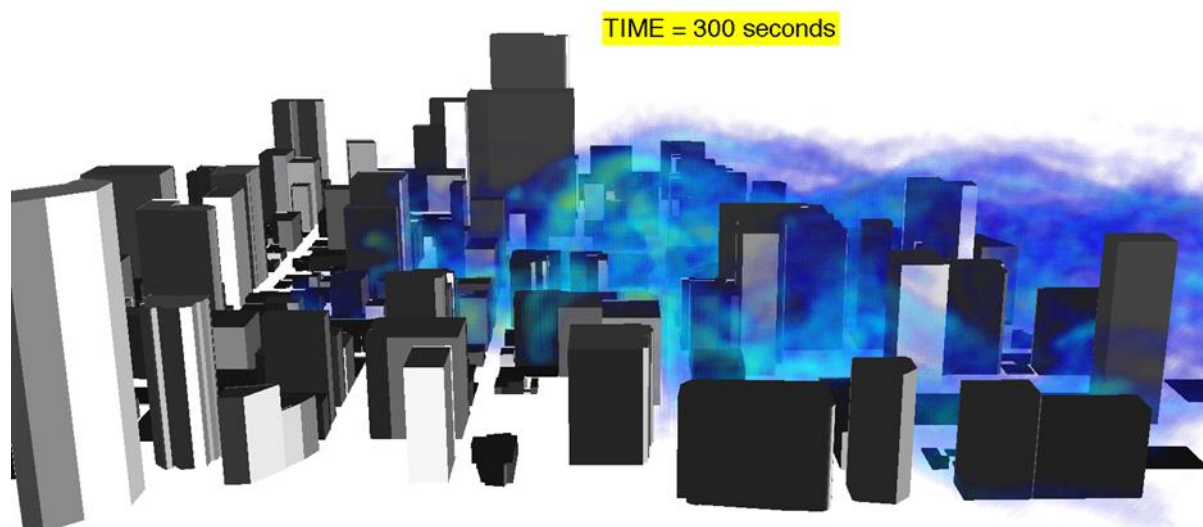


Figure 11 Vertical dispersion from the Chicago night LES run at 300 seconds after release (concentration scale is logarithmic; red is  $10^{-2}$  Ci/m<sup>3</sup> and deep blue is  $10^{-6}$  Ci/m<sup>3</sup>).

### 6.2.2 CEA results

Figure 12 shows 1 minute averaged concentration contours at street level (three-meter height) at different time steps for Chicago daytime case. Due to the local flow pattern near the source, there is upwind dispersion one block back on the right of North Michigan Avenue. Within 3 minutes, the plume is around 900 meters wide. Particles start to exit the domain after 5 minutes and are almost completely out of the domain after 20 minutes.

Figure 13 shows 1 minute averaged concentration contours at street level (three-meter height) at different time steps for the Chicago nighttime case. Within 3 minutes, the plume is around 800 meters wide. Particles start to exit the domain after 5 minutes and are almost completely out of the domain after 20 minutes, a quite similar time compared to the daytime case in spite of a higher nighttime inflow wind speed counter balanced by a lower wind speed at street level.

For both cases, the width of the cloud is about 500 meters at a distance of 600 meters from the release point. Despite different wind speed levels (also varying with the elevation above the ground) for the Chicago day and night case, particles tend to evacuate the urban district at the same time in both cases.

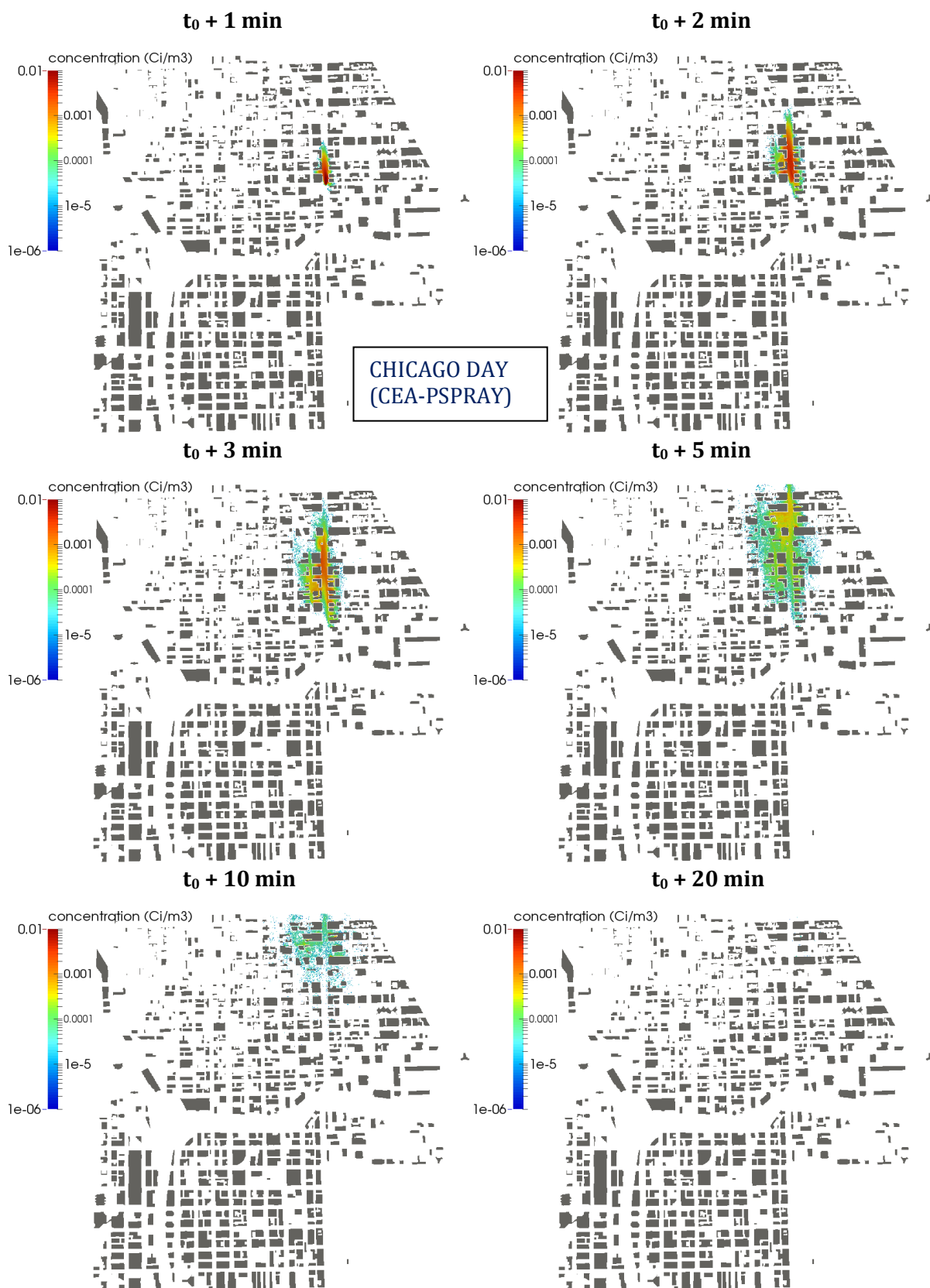


Figure 12 Chicago day PSPRAY air concentration in Ci/m<sup>3</sup> at different snapshots up to 20 minutes after release (scale is logarithmic; red is 10<sup>-2</sup> Ci/m<sup>3</sup> and deep blue is 10<sup>-6</sup> Ci/m<sup>3</sup>); from left to right, top to bottom, t=1 minute, 2 minutes, 3 minutes, 5 minutes, 10 minutes, and 20 minutes.

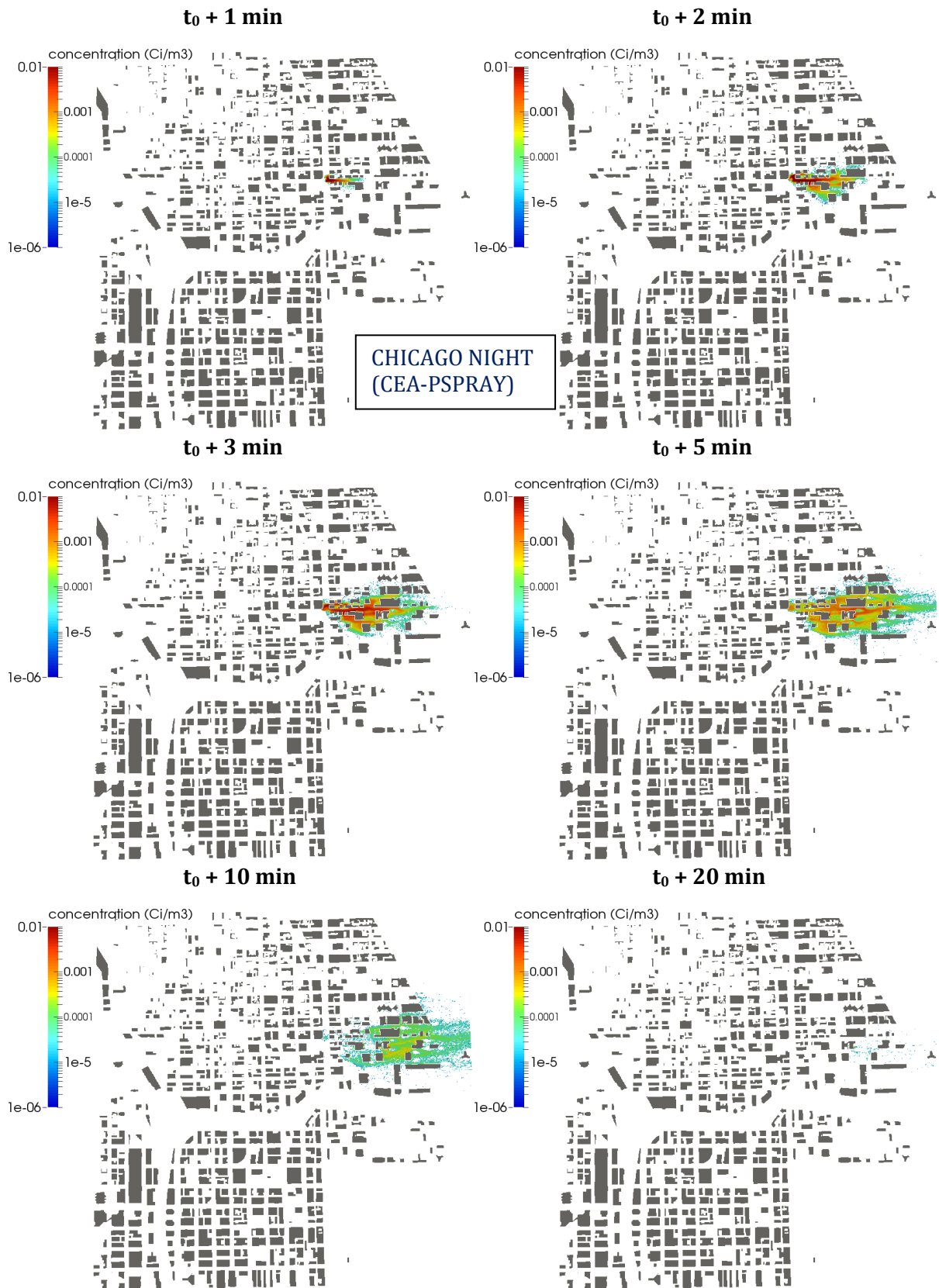


Figure 13 Chicago night PPSRAY air concentration in Ci/m<sup>3</sup> at different snapshots up to 20 minutes after release (scale is logarithmic; red is 10<sup>-2</sup> Ci/m<sup>3</sup> and deep blue is 10<sup>-6</sup> Ci/m<sup>3</sup>); from left to right, top to bottom, t=1 minute, 2 minutes, 3 minutes, 5 minutes, 10 minutes, and 20 minutes.

### 6.3 Chicago radiological exposure (CEA only)

Radiological exposure was evaluated by CEA using the volumetric activity concentration in the air and the activity concentration deposited on the ground (dry deposition). Total effective dose (TED) was computed taking account of three exposure pathways: inhalation, irradiation by the cloud shine, and irradiation by the ground shine. The details of the modeling are given in Appendix C.

Figure 14 and Figure 15 show TED for day and night cases for Chicago. For the modeled source term, the threshold of 50 mSv is passed on a small area around the emission point and downwind of some buildings for the day case, and over a bigger area for the night case.

For the day case, the footprint for the lower threshold of 10 mSv covers a large part of Michigan Avenue from the release point to a distance of about 600 meters. For the night case, the footprint of the 10 mSv threshold covers East Ohio Street from the release point to a distance of about 800 meters, and part of adjacent parallel streets.



**Figure 14 Chicago day total dose: PMSS (CEA) simulated TED in mSv; thresholds of 10 and 50 mSv illustrated in orange and red, respectively.**

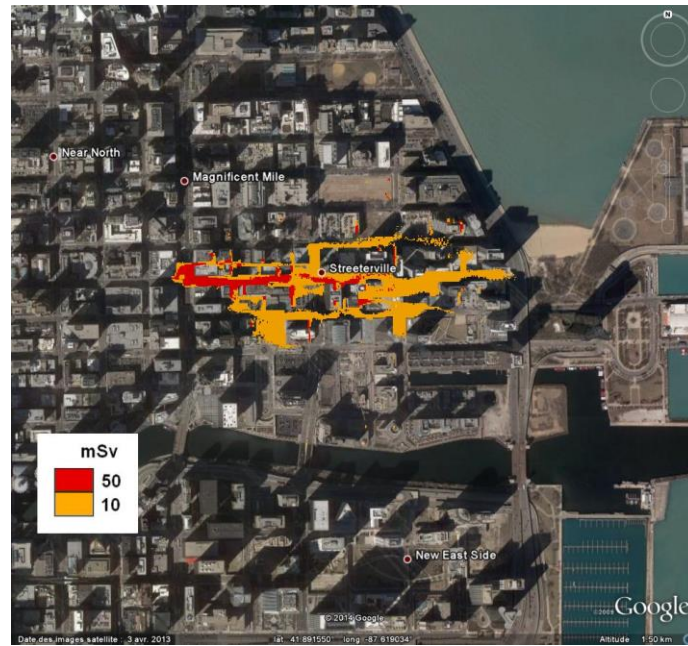


Figure 15

As shown in Figure 16 for Chicago day case, the dose by inhalation and the dose by irradiation due to the ground deposition integrated on four day are nearly the same for higher dose levels. The contribution of irradiation by the particle cloud is very weak compared to the other exposure pathways. The relative contributions to radiological exposure are the same for Chicago night case.

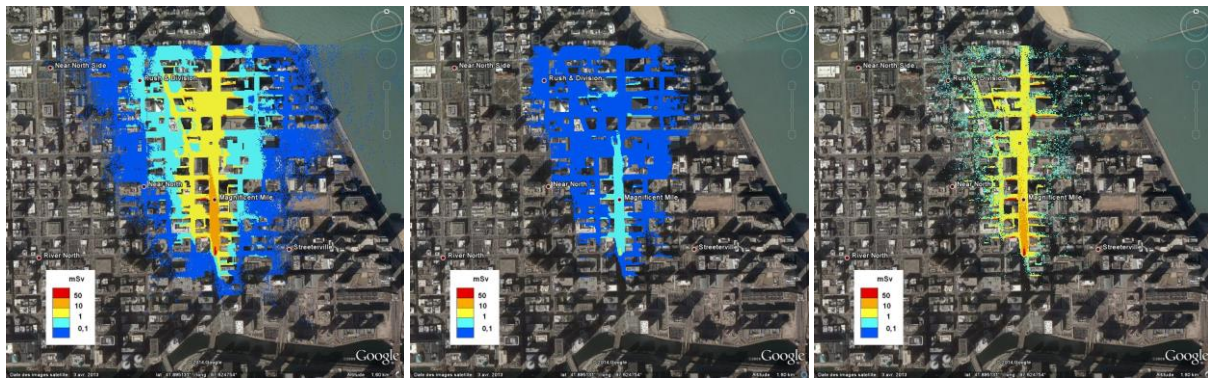


Figure 16 CEA simulated dose by inhalation (left), radiation by the cloud (middle) and radiation by the deposition on the ground (right) in mSv for Chicago day case; 50, 10, 1 and 0.1 thresholds illustrated in red, orange, yellow, light-blue, and dark-blue, respectively.

## 7 Computational results at local urban scale: Paris

As for Chicago, PMSS (mass-consistent diagnostic flow model and Lagrangian Particle Dispersion model) was used by CEA for the day and night Paris release scenarios. Fast-running (RANS) and high-fidelity (LES) model Aeolus runs were carried out by NARAC for the day and night scenarios in Paris. The metrics of interest were static wind fields and air concentration as a function of time.

### 7.1 Paris wind field (wind vector and velocity)

#### 7.1.1 LLNL results

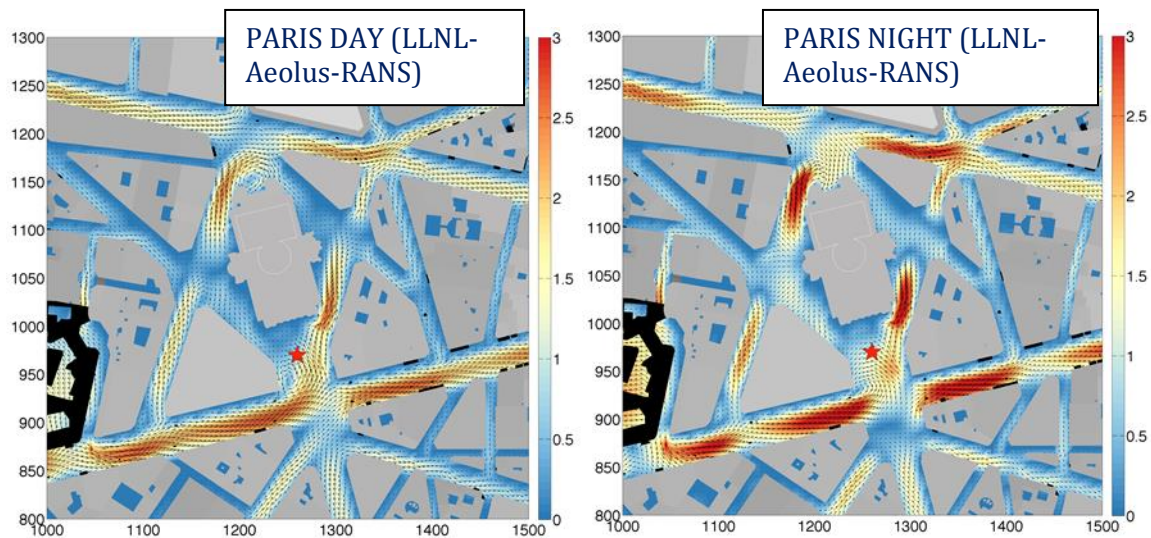


Figure 17 RANS Wind field for Paris day (left) and night (right). Wind speed is presented in m/s.

Figure 17 shows the time averaged wind speed magnitude and velocity vectors in a horizontal slice at street level for Paris. The inflow wind direction is same for both times, with higher velocity at night. The similarity in the wind direction causes the wind patterns at the street level to be similar, with the only change being the actual velocities observed. Along street channeling is clearly visible for both figures. Since the buildings and streets are not arranged in a grid, the level of alignment with inflowing wind that was seen in the Chicago case isn't possible for Paris. This factor combined with the absence of very tall buildings leads to a lack of highly influential divergence zones. Therefore, unlike Chicago, the higher inflow wind speed for the nighttime case leads to a correspondingly higher ground speed.

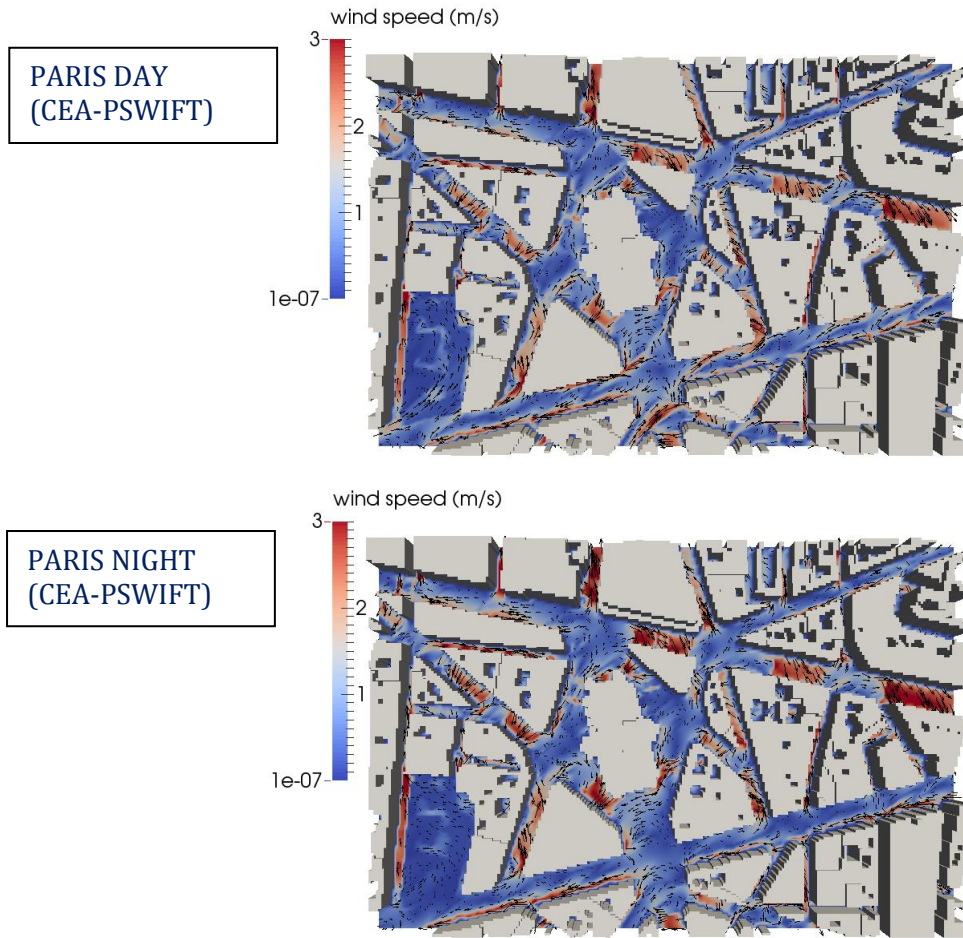


Figure 18 PSWIFT Wind field for Paris day (left) and night (right). Wind speed is presented in m/s.

### 7.1.2 CEA results

Figure 18 shows the time averaged wind speed magnitude and velocity vectors in a horizontal slice at street level for Paris. The inflow wind direction is same for both times, with higher velocity at night. The similarity in the wind direction causes the wind patterns at the street level to be similar. In spite of the fact that the inflow wind field is slightly higher for the nighttime compared to the daytime, the wind speed at street level is quite comparable for both cases. The wind speed may even be locally lower near the ground for nighttime.

## 7.2 Paris dispersion (volumetric activity concentration of $^{137}\text{Cs}$ in air)

### 7.2.1 LLNL results

The fast-running RANS mode was used with Aeolus to model both the daytime and nighttime scenarios for Paris. Figure 19 and Figure 20 show 1 minute averaged concentration contours at street level at different time steps for daytime and nighttime case respectively. Unlike the Chicago case, both scenarios exhibit very similar behavior for Paris. Due to the strong channeling in both cases, there is very little upwind dispersion near the source. In both cases, the plume is around 1,000 meters wide after 10 minutes. The plume starts to exit the domain slightly earlier for the nighttime case, which is consistent with its higher inflow wind speed.

A high fidelity LES run was carried out for the Paris nighttime case, with results shown in Figure 21. The voxels show instantaneous concentration level (blue-lower concentration and red-higher concentration). The channeling effects and the lateral spread are consistent with the RANS simulation. Figure 22 shows the vertical dispersion results for Paris. Considerably less vertical dispersion is seen here than in the Chicago case.

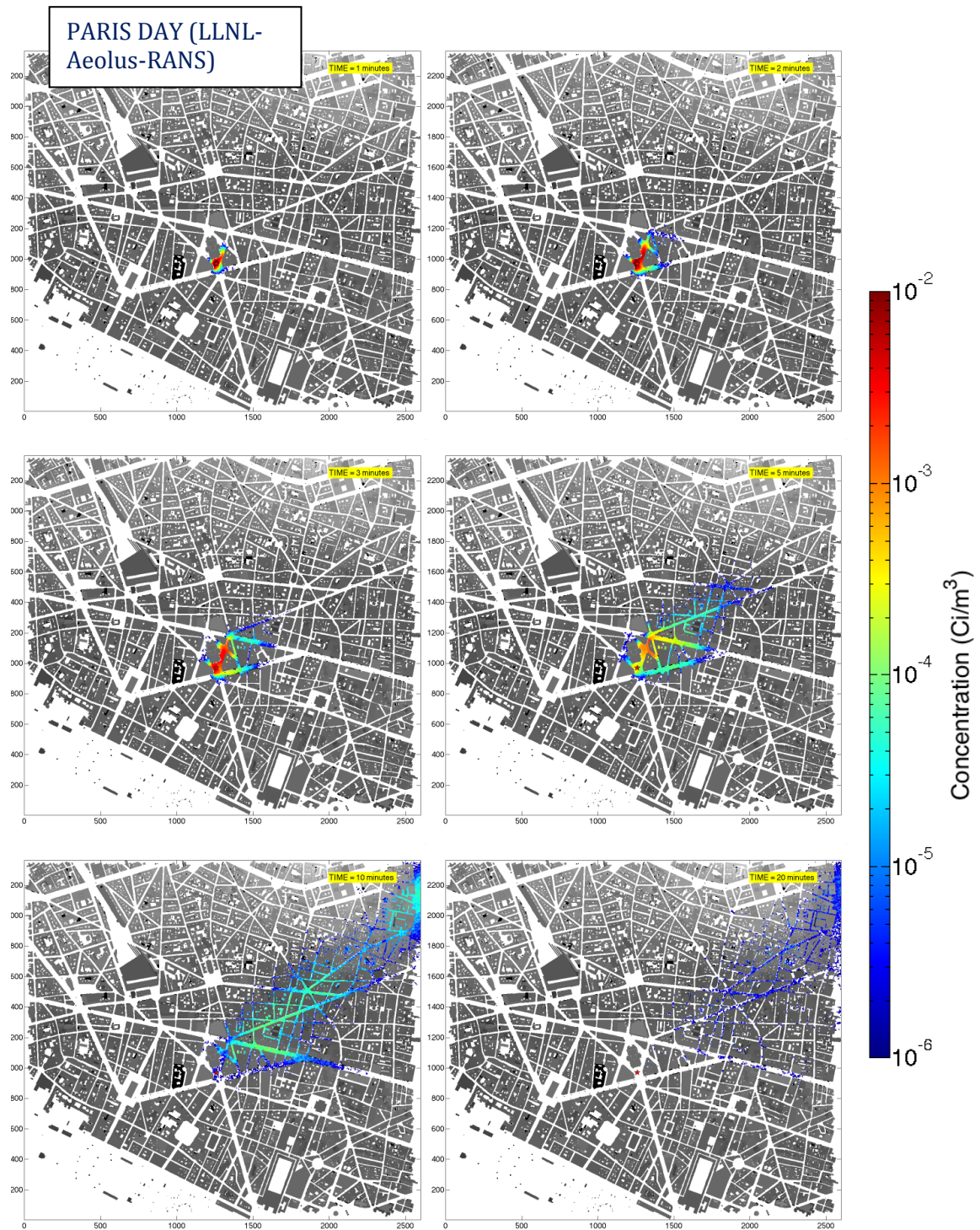


Figure 19 Paris day RANS snapshots in time up to 20 minutes after release; shown are air concentration plots (the scale is logarithmic; red is  $10^{-2}$  Ci/m<sup>3</sup> and deep blue is  $10^{-6}$  Ci/m<sup>3</sup>); from left to right, top to bottom,  $t = 1$  minute, 2 minutes, 3 minutes, 5 minutes, 10 minutes, and 20 minutes.

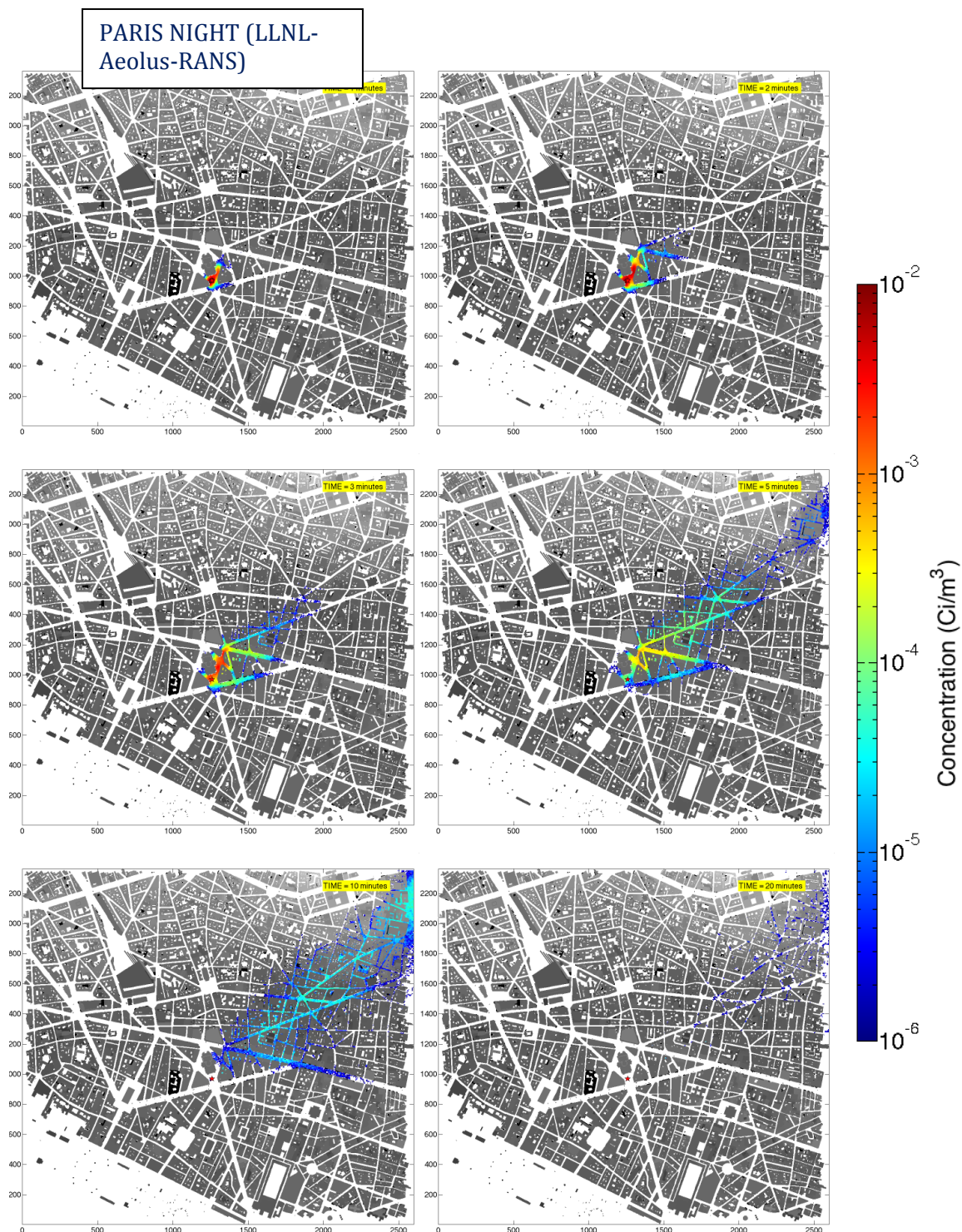


Figure 20 Paris night RANS snapshots in time up to 20 minutes after release; shown are air concentration plots (the scale is logarithmic; red is  $10^{-2}$  Ci/m<sup>3</sup> and deep blue is  $10^{-6}$  Ci/m<sup>3</sup>); from left to right, top to bottom,  $t = 1$  minute, 2 minutes, 3 minutes, 5 minutes, 10 minutes, and 20 minutes.

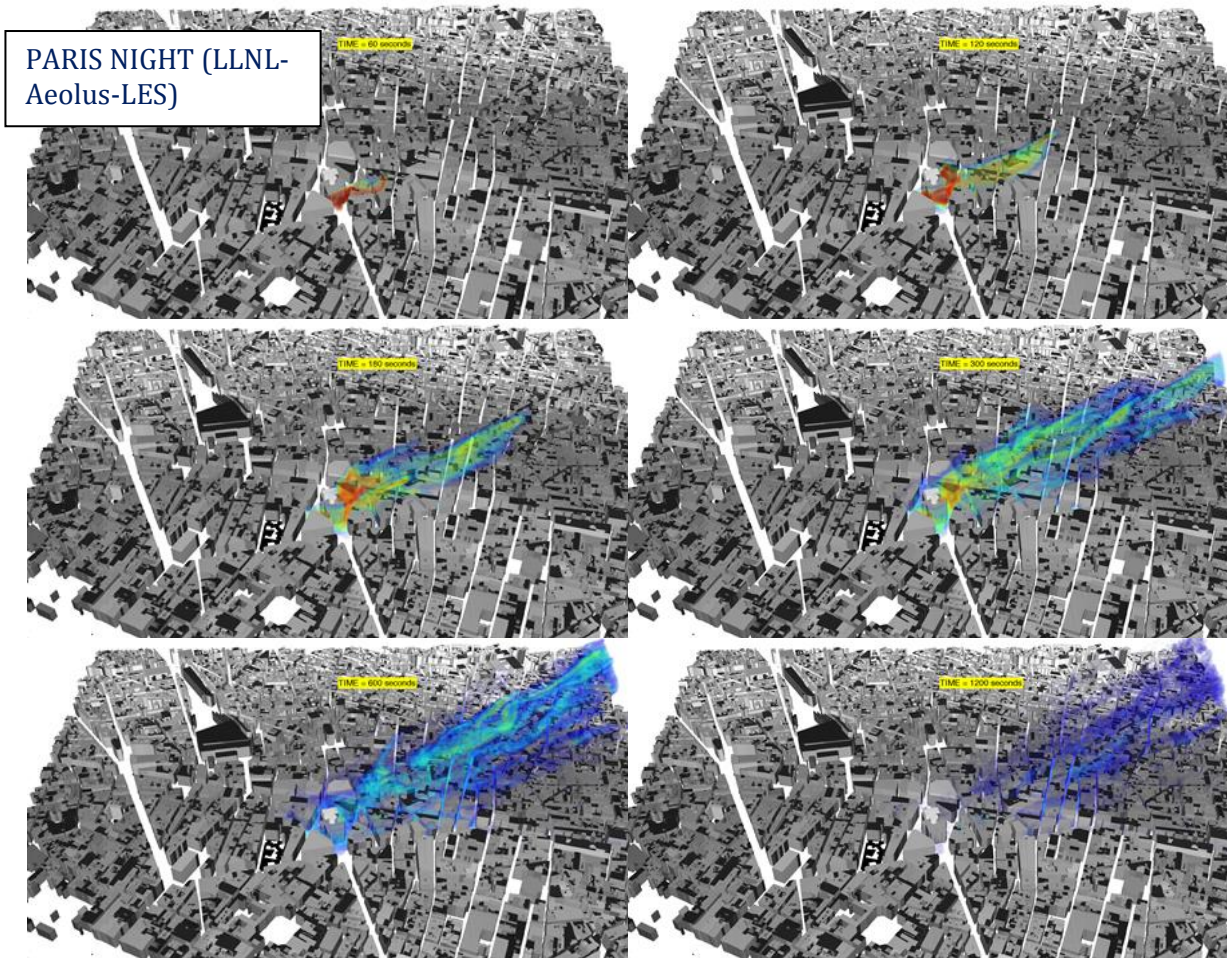


Figure 21 High fidelity LES simulation of nighttime Paris scenario snapshots in time up to 20 minutes after release; shown are air concentrations (the scale is logarithmic; red is  $10^{-2}$  Ci/m<sup>3</sup> and deep blue is  $10^{-6}$  Ci/m<sup>3</sup>); from left to right, top to bottom,  $t = 1$  minute, 2 minutes, 3 minutes, 5 minutes, 10 minutes, and 20 minutes.

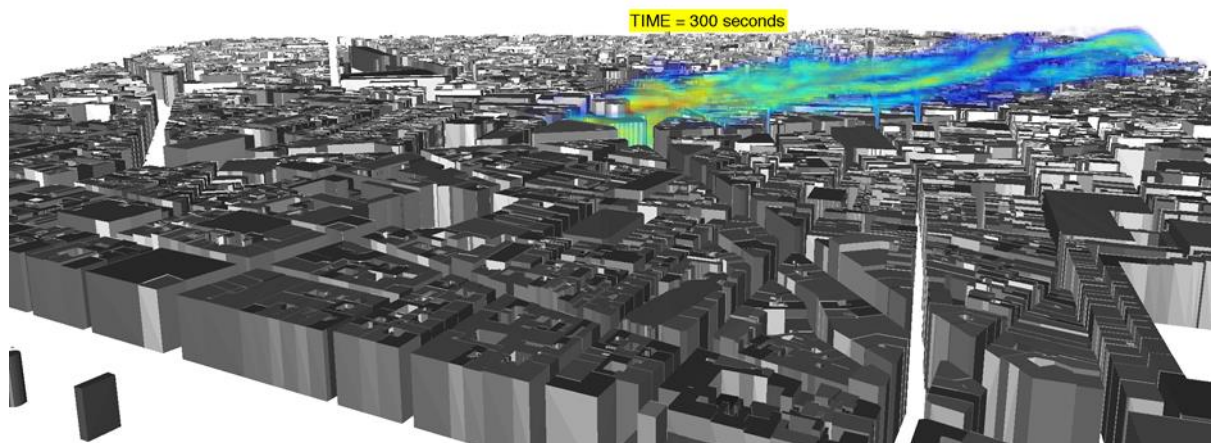


Figure 22 Paris nighttime LES simulation at 300 seconds after release with perspective to highlight the vertical dispersion; shown is air concentration (the scale is logarithmic; red is  $10^{-2}$  Ci/m<sup>3</sup> and deep blue is  $10^{-6}$  Ci/m<sup>3</sup>).

### 7.2.2 CEA results

Figure 23 shows 1 minute averaged concentration contours at street level (three-meter height) at different time steps for Paris daytime case. Near the source, there is noticeable upwind dispersion in the “boulevard des Capucines” for a distance of about 150 meters. Within 3 minutes, the plume is around 600 meters wide. Particles are almost completely out of the domain after 20 minutes.

Figure 24 shows 1 minute averaged concentration contours at street level (three-meter height) at different time steps for Paris nighttime case. Near the source, the same upwind dispersion can be observed as for the daytime case. Within 3 minutes, the plume is around 300 meters wide. While an exit time slightly longer than for the daytime, particles are almost completely out of the domain after 20 minutes.

For both Paris cases, the footprint of the cloud matches the wind direction. Despite a slightly higher inflow wind speed at night, the movement of the cloud inside the urban canopy is a marginally faster for the day case (e.g., similar footprints are observed at  $t_0 + 2$  min for the day case and  $t_0 + 3$  min for the night case). This could be explained by the local flow configuration in the streets near the release location counter balancing the wind speed at higher elevations.

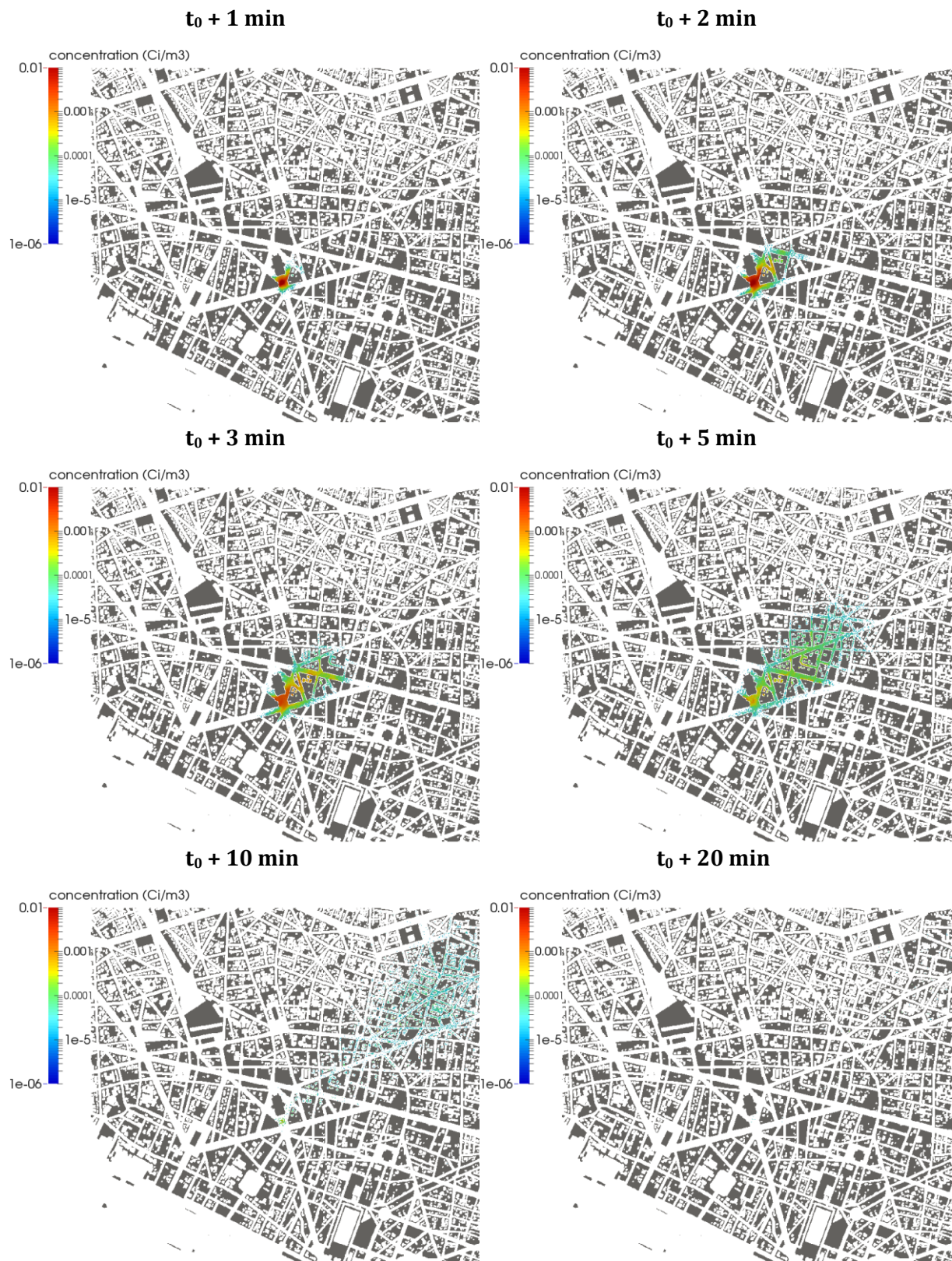


Figure 23 Paris day PSPRAY snapshots in time up to 20 minutes after release; shown are air concentration plots (the scale is logarithmic; red is  $10^{-2} \text{ Ci/m}^3$  and deep blue is  $10^{-6} \text{ Ci/m}^3$ ); from left to right, top to bottom,  $t = 1 \text{ minute}$ ,  $2 \text{ minutes}$ ,  $3 \text{ minutes}$ ,  $5 \text{ minutes}$ ,  $10 \text{ minutes}$ , and  $20 \text{ minutes}$ .

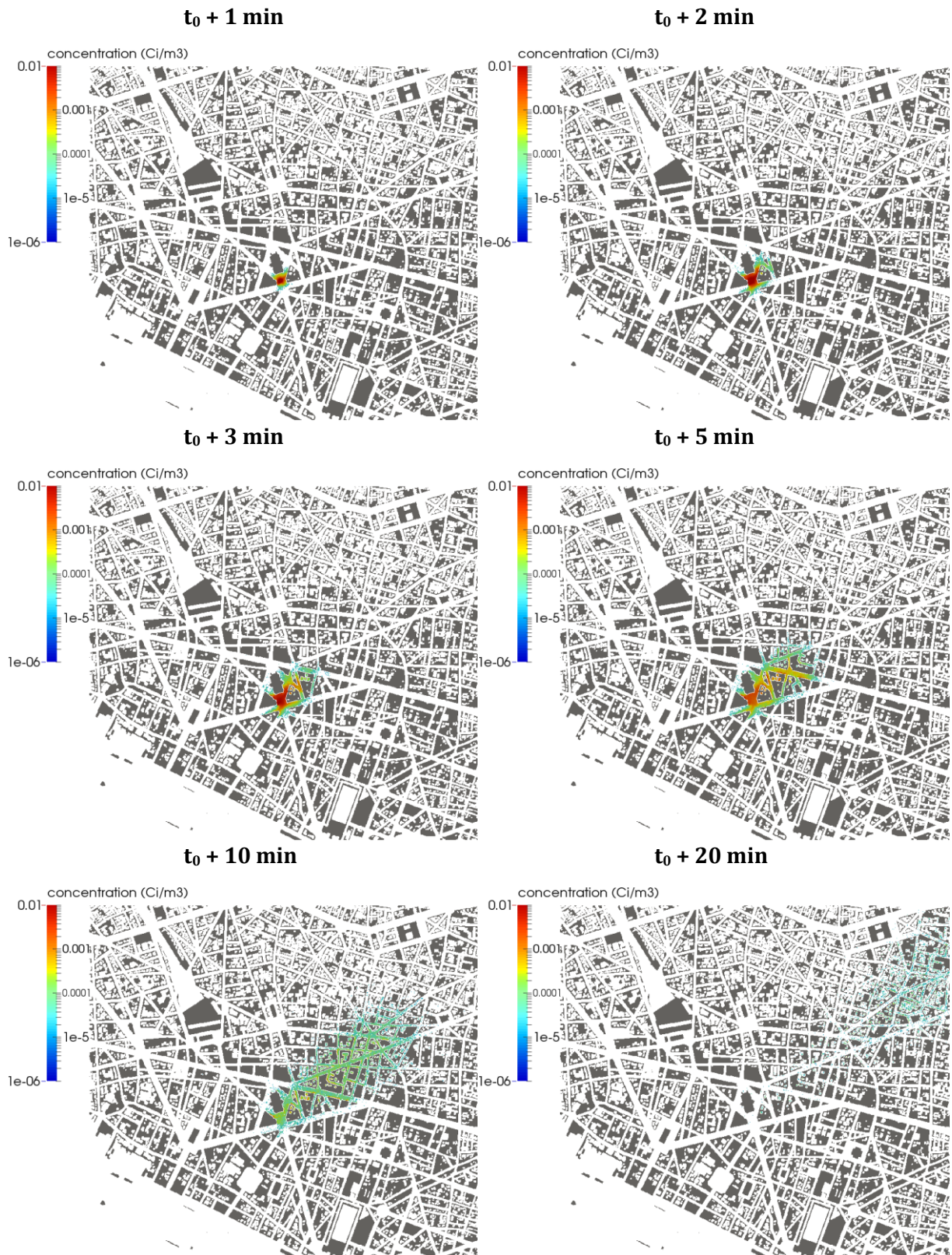


Figure 24 Paris night PSPRAY snapshots in time up to 20 minutes after release; shown are air concentration plots (the scale is logarithmic; red is  $10^{-2} \text{ Ci/m}^3$  and deep blue is  $10^{-6} \text{ Ci/m}^3$ ); from left to right, top to bottom,  $t = 1$  minute, 2 minutes, 3 minutes, 5 minutes, 10 minutes, and 20 minutes.

### 7.3 Paris exposure (CEA only)

Figure 25 and Figure 26 show the total effective dose (TED) for day and night cases for Paris. The area where inhalation dose exceeds the 50 mSv threshold covers the space directly in front of the Opera Garnier, some areas inside the streets network downwind of the release point and, in the night case, upwind the release point. The area where inhalation dose exceeds the 10 mSv threshold is more extensive (despite its patchy appearance) for the night case than for the day due to a longer residence time of the cloud inside the urban canopy.

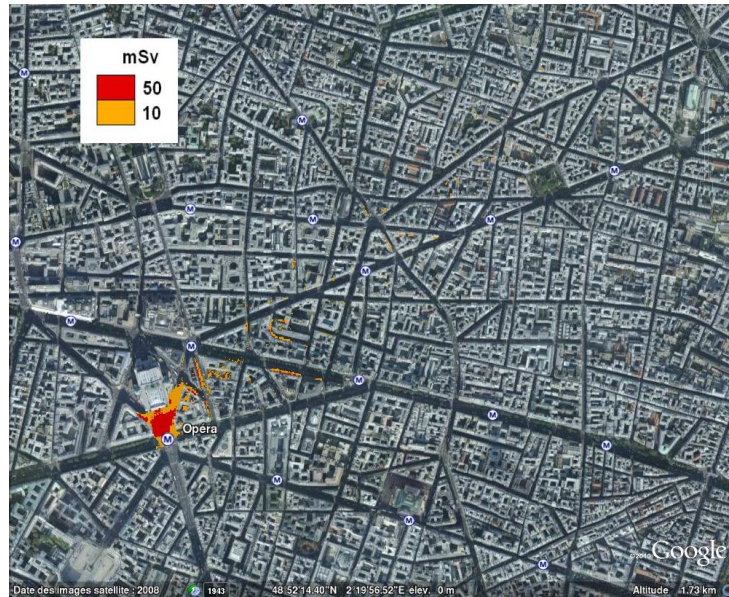


Figure 25 Paris day total dose: PMSS (CEA) simulated TED in mSv; thresholds of 10 and 50 mSv illustrated in orange and red, respectively.

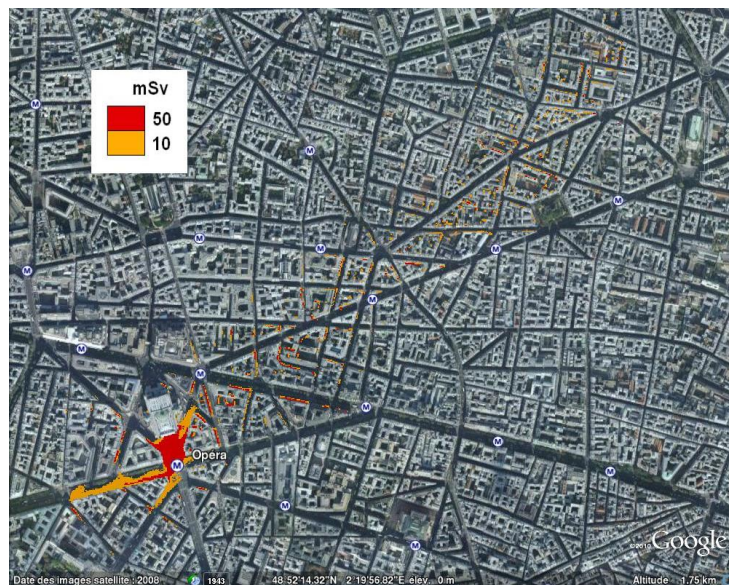


Figure 26 Paris day total dose: PMSS (CEA) simulated TED in mSv; thresholds of 10 and 50 mSv illustrated in orange and red, respectively.

## 8 Computational results at regional scale using the rawinsondes

A large release of 500,000 Ci over a six hour time period (Table 6) for the two Chicago release scenarios is considered both with a simple diagnostic wind profile from rawinsonde observations as a WRF wind forecast described in Section 9. Metrics of interest included the ground-level airborne activity concentration of Cs-137 at different snapshots in time and total integrated dose over four days. This four-day duration was chosen as a typical short-term dose guideline. Since these simulations are intended primarily to illustrate the difference between simplistic and sophisticated (WRF) meteorology inputs, the Paris scenarios were not included.

### 8.1 Dispersion (volumetric activity air concentration of Cs-137)

#### 8.1.1 LLNL results

LODI modeled the release and fate of the radiological material for four days. Air concentrations were recorded at all locations hourly over the four day time period. Figure 27 and Figure 28 illustrate the 1 and 6 hour air concentrations as predicted by LODI based on the single profile observation meteorology (Table 5) for the regional scale models of Chicago for the day and night cases, respectively. Unlike the urban scale case, this is a continuous release, hence, the high degree of similarity for the 1 and 6 hour plumes for both cases. The uniform input meteorology results in very simple Gaussian type plumes, as expected.

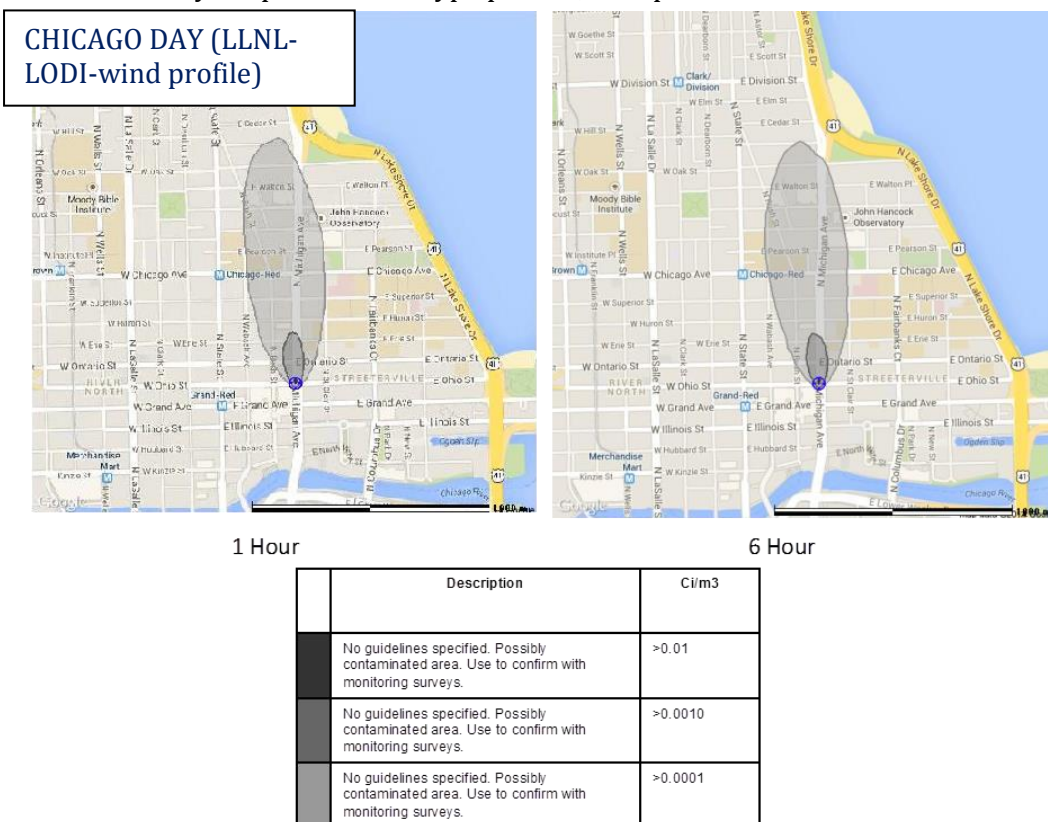


Figure 27 Uniform meteorology based dispersion predictions at 1 and 6 hours for the regional scale Chicago daytime scenario. Note the Gaussian nature of the plumes and constant concentration due to the time-invariant release and wind field. Contours are air concentration exceedance levels in units of Ci/m<sup>3</sup>.

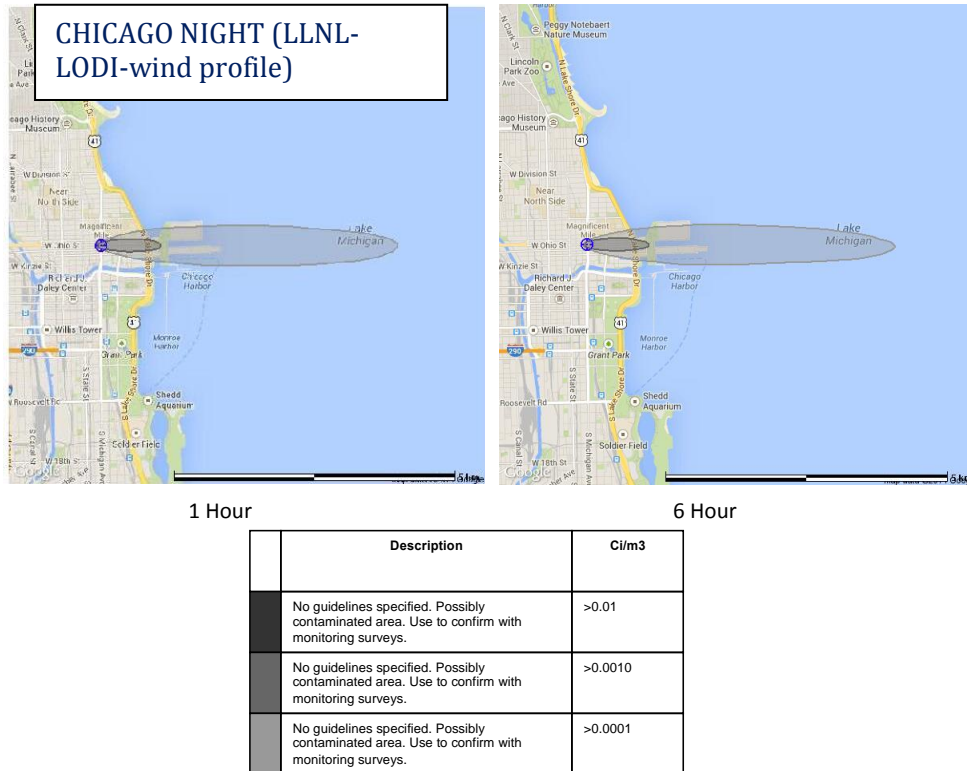


Figure 28 Uniform meteorology based dispersion predictions at 1 and 6 hours for the regional scale Chicago nighttime scenario. Contours are air concentration exceedance levels in units of Ci/m<sup>3</sup>.

### 8.1.2 CEA results

PSPRAY modeled the release and fate of the radiological material for four days. Air concentrations were recorded at all locations hourly over the entire time period. The meteorology used as input to PSPRAY was computed by PSWIFT based on the canned meteorology (Table 5) and took into account the influence of topography, roughness length and atmospheric stability on wind flow.

Figure 29 and Figure 30 show the 1 and 6 hour air concentrations predicted by PSPRAY for the Chicago day and night cases, respectively. Unlike the urban scale case, the release is continuous, causing the high degree of similarity for the 1 and 6 hour plumes for both cases. For the day case, the distance from the release point where concentration is higher than 0.0001 Ci/m<sup>3</sup> does not exceed 1500 meters at 1 hour or 6 hours. For the night case, this distance does not exceed 500 meters at 1 hour and 7000 meters at 6 hours.

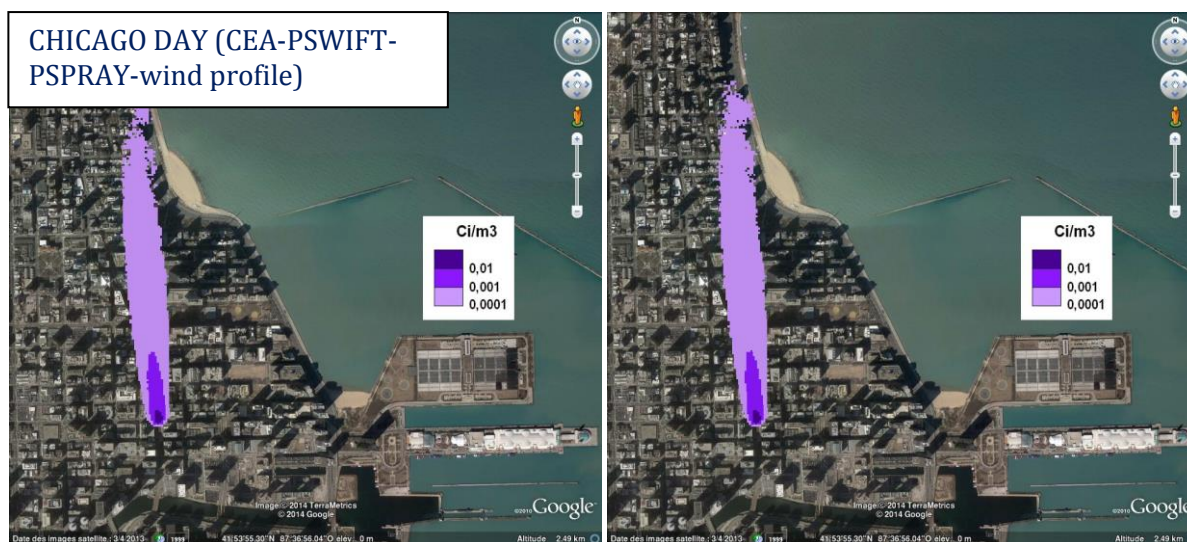


Figure 29 Uniform meteorology based dispersion predictions at 1 and 6 hours for the regional scale Chicago daytime scenario. Contours are air concentration exceedance levels in  $\text{Ci}/\text{m}^3$ .

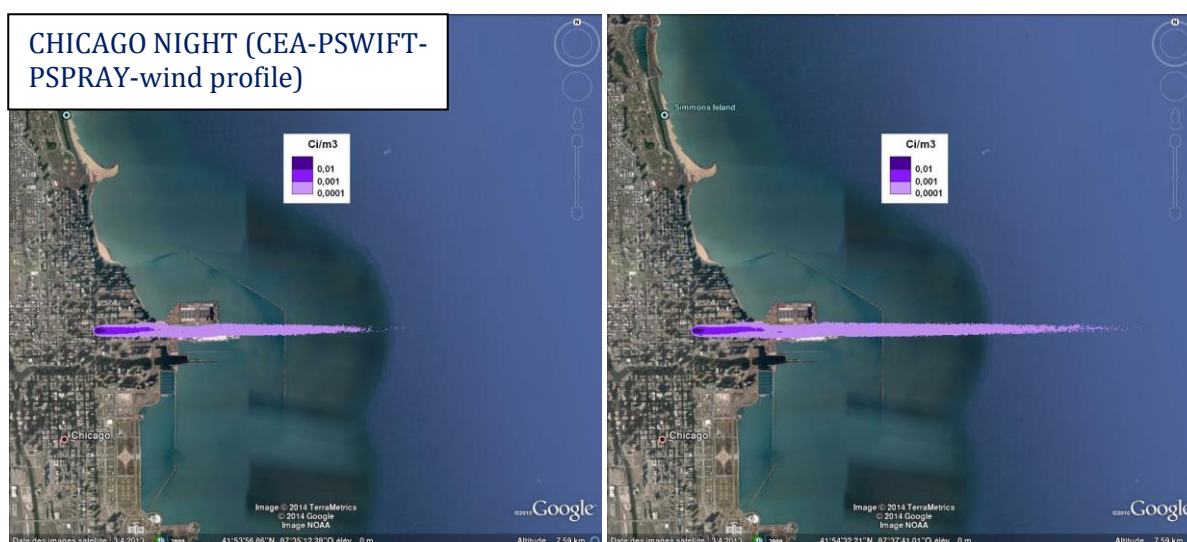


Figure 30 Uniform meteorology based dispersion predictions at 1 and 6 hours for the regional scale Chicago nighttime scenario. Contours are air concentration exceedance levels in  $\text{Ci}/\text{m}^3$ .

## 8.2 Radiological exposure assessment (Total Effective Dose Equivalent)

### 8.2.1 LLNL results

Figure 31 shows the four day (96 hour) dose predictions for Chicago day and night simulations using canned meteorology as input. Contours are given for the  $>1$  rem ( $>10$  mSv) and  $>5$  rem ( $>50$  mSv) total effective dose (TED per ICRP Publication 66<sup>9</sup>). As with the concentration predictions, using simplified meteorology with a continuous release leads to a simple Gaussian dose pattern.

<sup>9</sup> (ICRP, 1994)

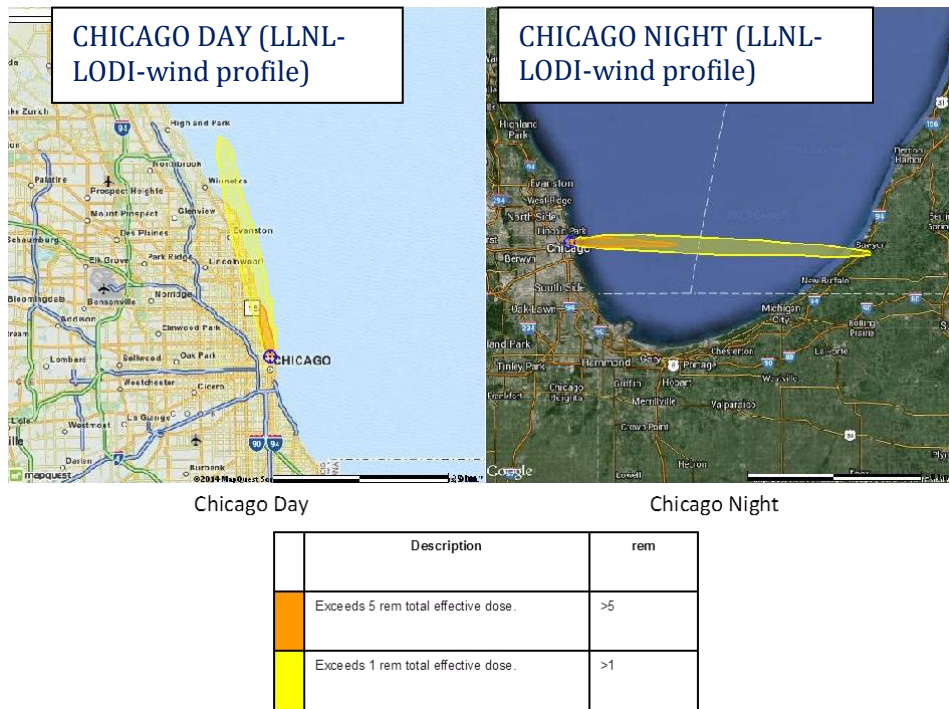


Figure 31 Uniform meteorology based cumulative 96 hour dose prediction for regional scale Chicago scenarios. Contours are TED exceedance levels in units of rem.

### 8.2.2 CEA Results

Figure 32 shows the four day (96 hours) dose predictions for Chicago day and night simulations using canned meteorology processed by PSWIFT as input. Contours are given for values >10 mSv (>1 rem) and >50 mSv (>5 rem) TED computed as described in Section 6.3.1. As with the concentration predictions, using simplified meteorology with a continuous release leads to the dose pattern looking like a Gaussian plume.

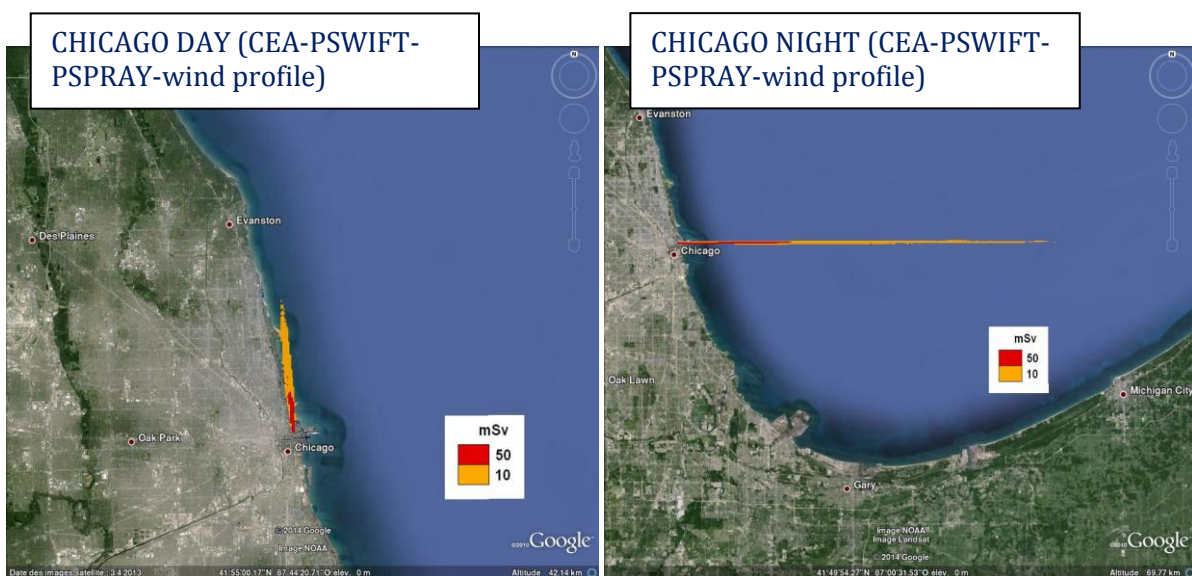


Figure 32 Uniform meteorology based cumulative 96 hour dose prediction for regional scale Chicago scenarios. Contours are TED exceedance levels in mSv.

## 9 Computational results at regional scale using WRF wind field

Releases identical to those from Section 8 were then considered with high-resolution WRF forecasts as input. Again, the metrics of interest were air concentration at 1 and 6 hours and dose at four days. For these simulations, both Chicago and Paris scenarios were considered, as described in Table 7.

### 9.1 Dispersion (volumetric activity air concentration of Cs-137)

#### 9.1.1 LLNL results

Figure 33 and Figure 34 show the 1 and 6 hour air concentration results for the Chicago day and night scenarios with WRF wind forecasts used as meteorological input. For the daytime case the plume has a simple Gaussian shape similar to the uniform meteorology case (Figure 27 and Figure 28), but the plume direction is northeast rather than north. Recall that these cases are for different simulated days, so the plume directions should not be directly compared. The differences are greater for the nighttime case (Figure 28).

Figure 35 and Figure 36 show the equivalent 1 and 6 hour air concentration results for Paris. While there are no canned meteorology simulations for comparison in this case, the 1 and 6 hour time points show changes in wind direction for both the day and night scenarios. This behavior would not be captured under the simplified meteorology situation, and will have an impact on final deposition and dose predictions.

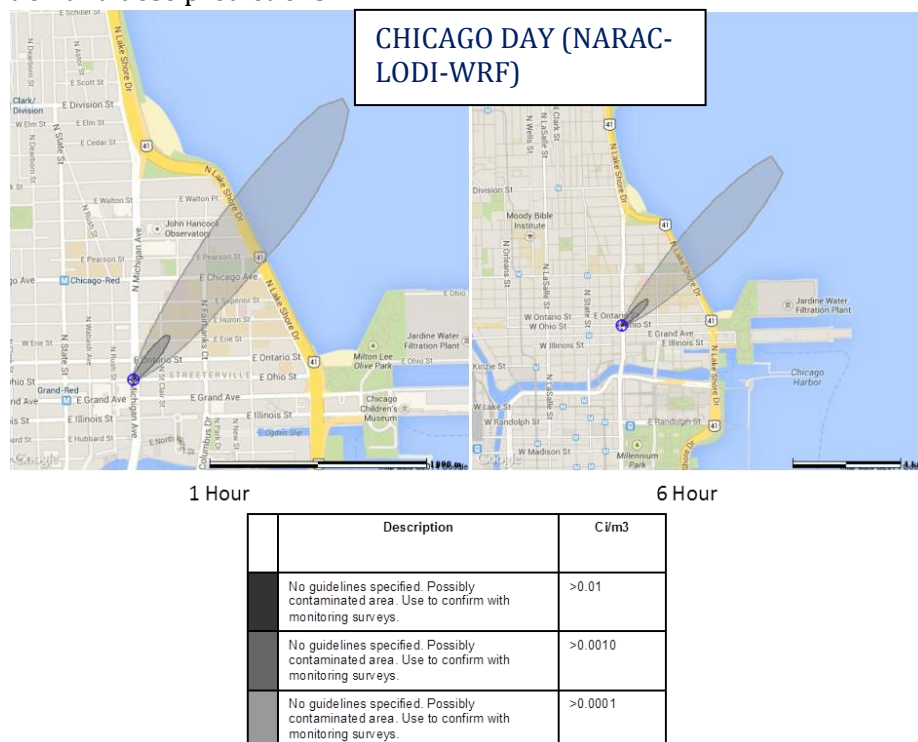
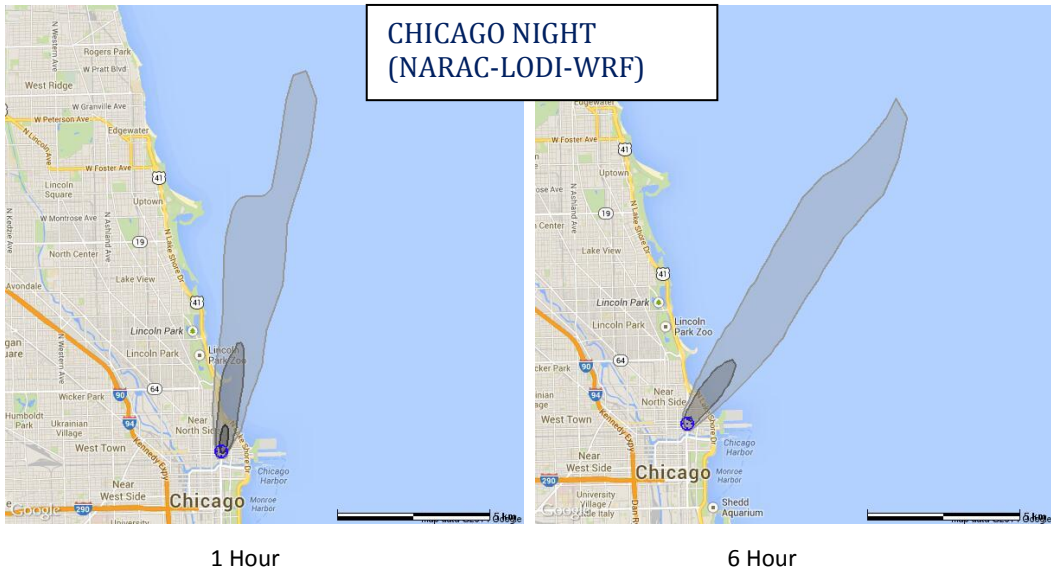


Figure 33 WRF forecast based dispersion predictions at 1 and 6 hours for the regional scale Chicago daytime scenario. Contours are air concentration exceedance levels in units of Ci/m<sup>3</sup>.



	Description	Ci/m3
	No guidelines specified. Possibly contaminated area. Use to confirm with monitoring surveys.	>0.0010
	No guidelines specified. Possibly contaminated area. Use to confirm with monitoring surveys.	>0.0001
	No guidelines specified. Possibly contaminated area. Use to confirm with monitoring surveys.	>1.00E-5

Figure 34 WRF forecast based dispersion predictions at 1 and 6 hours for the regional scale Chicago nighttime scenario. Contours are air concentration exceedance levels in units of Ci/m<sup>3</sup>.



	Description	Ci/m3
	No guidelines specified. Possibly contaminated area. Use to confirm with monitoring surveys.	>0.01
	No guidelines specified. Possibly contaminated area. Use to confirm with monitoring surveys.	>0.0010
	No guidelines specified. Possibly contaminated area. Use to confirm with monitoring surveys.	>0.0001

Figure 35 WRF forecast based dispersion predictions at 1 and 6 hours for the regional scale Paris daytime scenario. Contours are air concentration exceedance levels in units of Ci/m<sup>3</sup>.



Figure 36 WRF based dispersion predictions at 1 and 6 hours for the regional scale Paris nighttime scenario. Contours are air concentration exceedance levels in units of Ci/m<sup>3</sup>.

### 9.1.2 CEA results

Figure 37 and Figure 38 show the 1 and 6 hour air concentration results computed by PSPRAY for the Chicago day and night scenarios with WRF wind forecasts used as meteorological input to PSWIFT and PSWIFT turbulent wind field utilized as input to PSPRAY. For the daytime case, 1 hour after the beginning of the run, the plume has a simple Gaussian shape similar to the uniform meteorology case (Figure 29), but has spread over a longer distance and the plume direction is northeast rather than north. Six hours after the beginning of the run, the plume direction is similar, but the 10<sup>-4</sup> Ci/m<sup>3</sup> contour is observed on a longer distance. Plume dispersal for the nighttime case is similar (Figure 30) with the plume direction extending to the northeast, instead of due east. For the nighttime case, the plume shape is more extended and less diffuse when using the detailed WRF wind field.

Figure 39 and Figure 40 show the equivalent 1 and 6 hour air concentration results for Paris. While there are no canned meteorology simulations for direct comparison in this case, the 1 and 6 hour time points show changes in wind direction for both the day and night scenarios. This behavior would not be captured under the simplified meteorology situation, and will have an impact on final deposition and dose predictions. As wind speed is lower for the Paris cases compared to the Chicago cases, the corresponding plumes are wider.

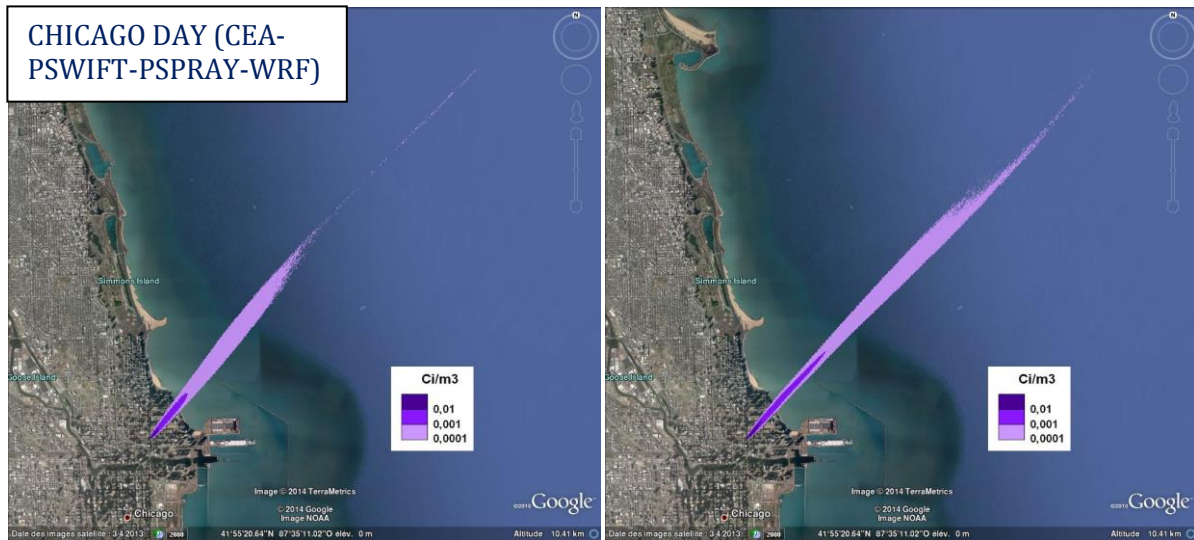


Figure 37 WRF forecast based dispersion predictions at 1 and 6 hours for the regional scale Chicago daytime scenario. Contours are air concentration exceedance levels in units of  $Ci/m^3$ .

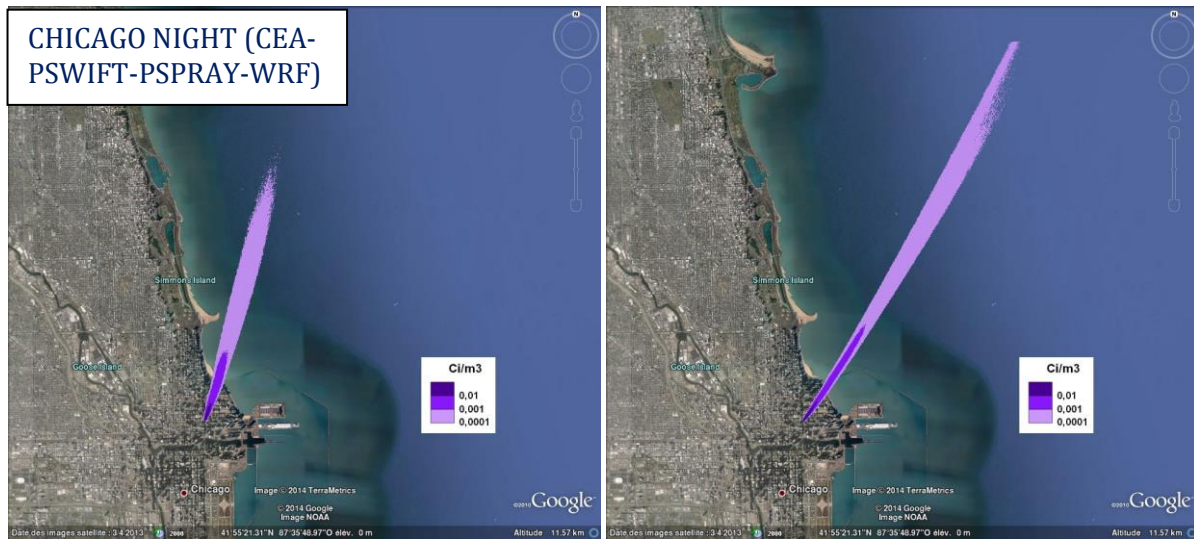


Figure 38 WRF forecast based dispersion predictions at 1 and 6 hours for the regional scale Chicago nighttime scenario. Contours are air concentration exceedance levels in units of  $Ci/m^3$ .



Figure 39 WRF forecast based dispersion predictions at 1 and 6 hours for the regional scale Paris daytime scenario. Contours are air concentration exceedance levels in units of  $Ci/m^3$ .



Figure 40 WRF forecast based dispersion predictions at 1 and 6 hours for the regional scale Paris nighttime scenario. Contours are air concentration exceedance levels in units of  $\text{Ci}/\text{m}^3$ .

## 9.2 Radiological exposure assessment (Total Effective Dose Equivalent)

### 9.2.1 LLNL Results

Figure 41 and Figure 42 show the TED for the first 96 hours post release for Chicago and Paris respectively. Contours are shown for exposure greater than 1 rem (10 mSv) and greater than 5 rem (50 mSv). Note the differences between these contours and those based on canned meteorology in Section 8.2.1 (Figure 31). While plume direction should not be directly compared, the overall plume shapes for the WRF simulations are more complex than those from the simplified wind case based exclusively on rawinsonde data. The Paris night scenario, in particular, shows indications of a shift in wind direction during the release period, highlighting the importance of capturing spatially and temporally varying winds as well as quality forecast data.

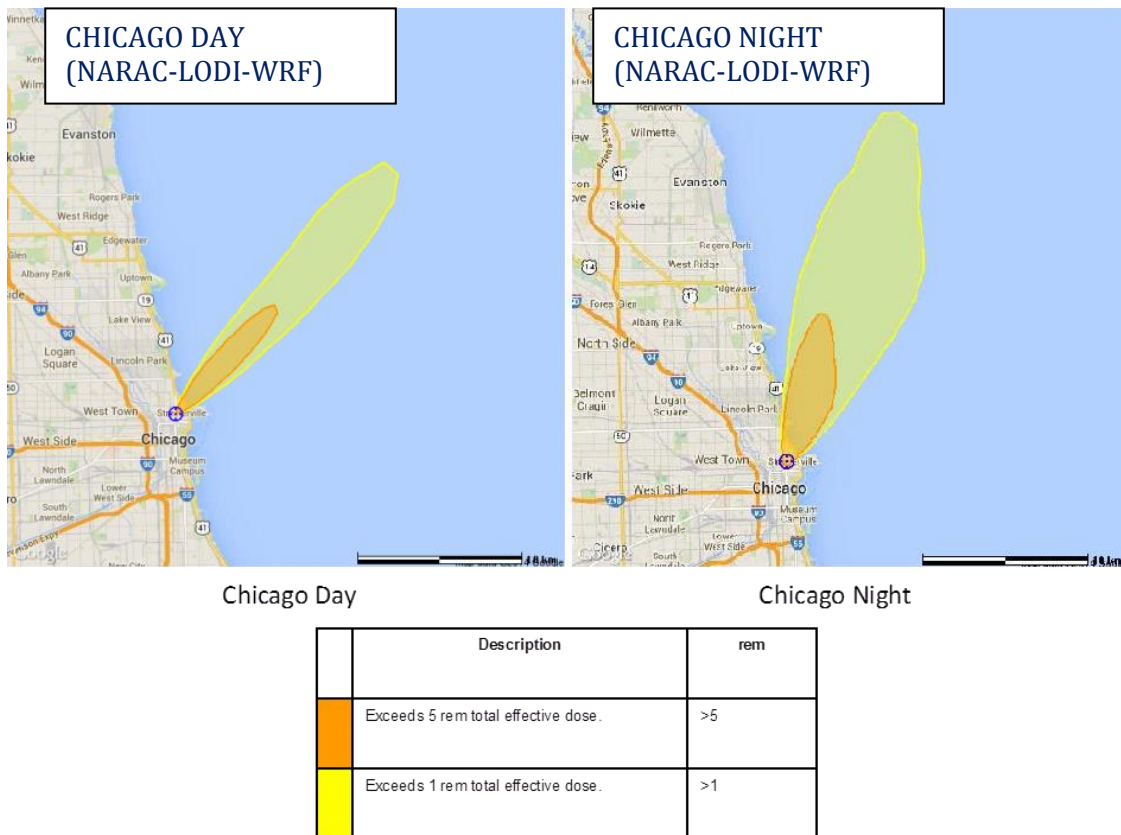


Figure 41 WRF forecast based 96 hour cumulative dose prediction for regional scale Chicago scenarios. Contours are TED exceedance levels in units of rem.

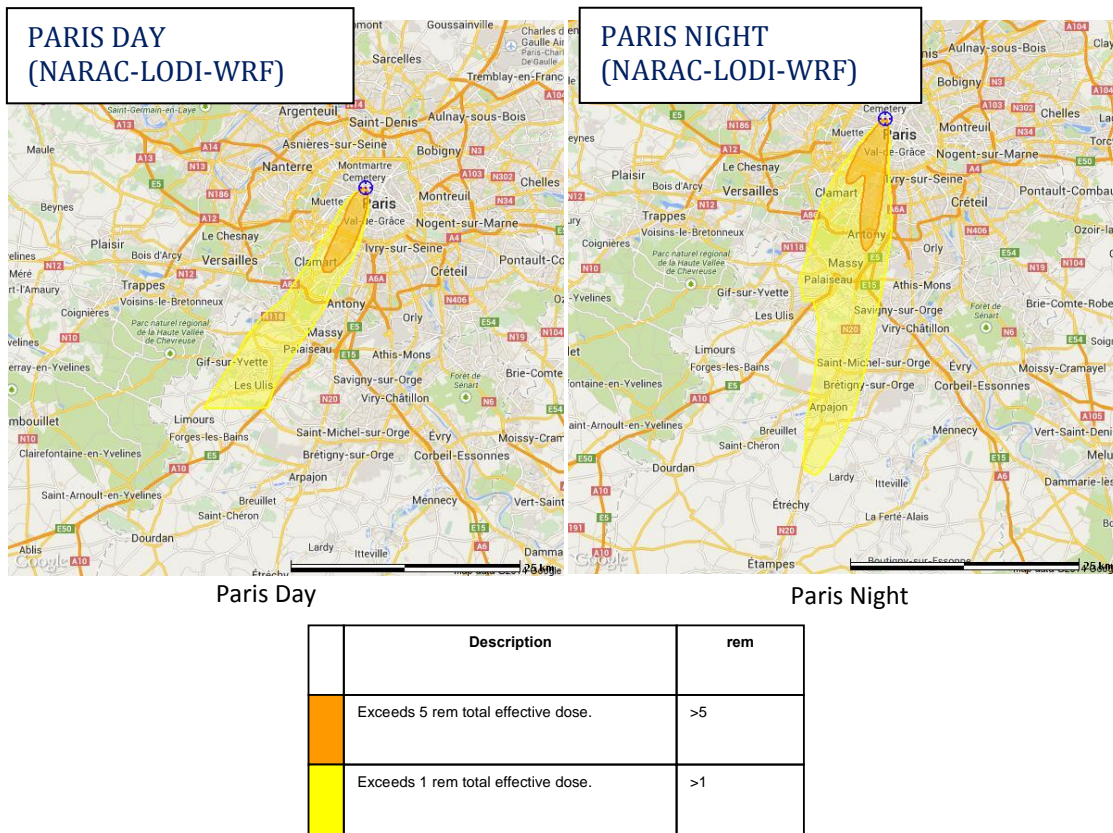


Figure 42 WRF forecast based 96 hour cumulative dose prediction for regional scale Paris scenarios. Contours are TED exceedance levels in units of rem.

9.2.2 CEA Results

Figure 43 and Figure 44 show the total effective dose (TED) for Chicago and Paris respectively. Dose contours are given for values >10 mSv (>1 rem) and >50 mSv (>5 rem). Note the differences between these contours and those based on canned meteorology processed by PSWIFT in Section 8.2.2 (Figure 32). Due to changing wind (in direction and in speed) and changing conditions for turbulence, the overall shape of the area where the TED exceeds 10 mSv or 50 mSv can be extremely different from the prediction based on a single meteorological observation. As an example, for the Paris night case, the non-Gaussian shape of the area where the TED is greater than 10 mSv clearly indicates a shift in wind direction during the release period. The influence of topography and the presence of enclosed valleys manifest as discontinuities in the shape of the plume.

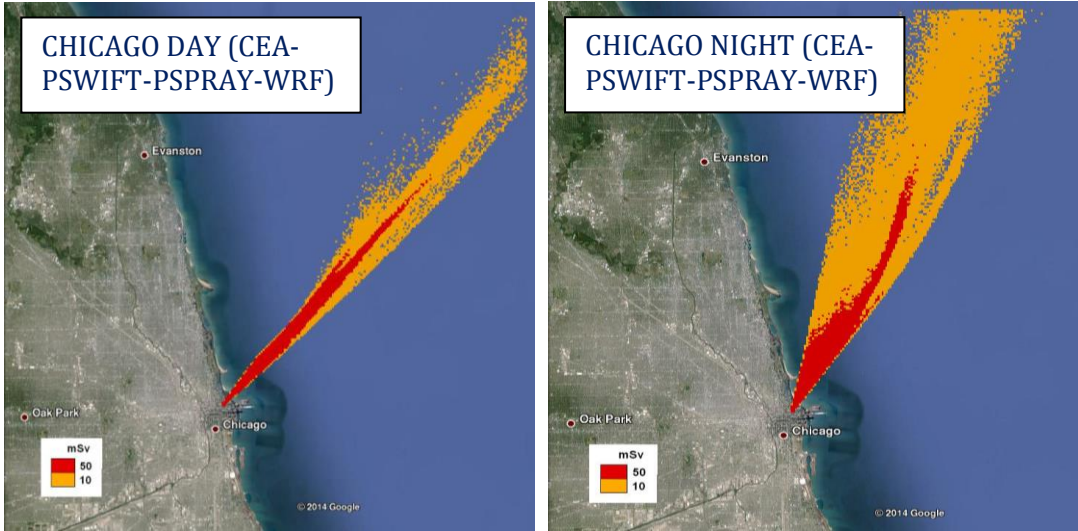


Figure 43 WRF forecast based 96 hour cumulative dose prediction for regional scale Chicago scenarios. Contours are TED exceedance levels in 10 and 50 mSv (orange and red, respectively).

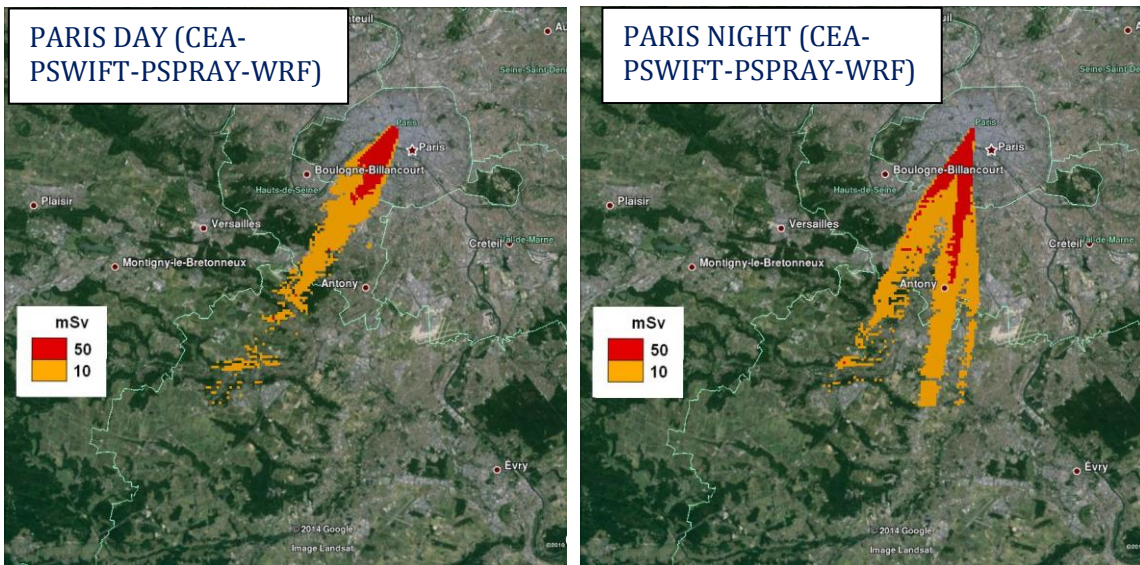


Figure 44 WRF forecast based 96 hour cumulative dose prediction for regional scale Paris scenarios. Contours are TED exceedance levels in 10 and 50 mSv (orange and red, respectively).

## 10 Modeling Discussion

In this table top exercise, LLNL and CEA compared each other's flow and dispersion models. The goal of the comparison is to facilitate the exchange of knowledge, capabilities, and practices. Two modeling approaches were examined, a regional scale modeling approach, appropriate for simple terrain and/or very large releases, and an urban scale modeling approach, appropriate for small releases in a city environment. The joint CEA/LLNL team made the following high level observations:

- At the regional scale, the CEA and LLNL modeling results were similar as the meteorological data (either vertical profiles given by rawinsondes or WRF wind fields) were strictly the same and both organizations used Lagrangian Particle Dispersion Models (LLNL's LODI and CEA's PSPRAY).
- At the urban scale, both LLNL and CEA approaches combine a turbulent flow field model and a LPDM able to simulate urban environments in Chicago and Paris. While there is a commonality in the use of a Lagrangian dispersion model, both lab's took significantly different approaches to modeling air flow. The CEA approach is a 3D mass-consistent diagnostic flow model using Röckle type flow zones around the buildings, while the LLNL approaches are fully resolved RANS and LES Navier-Stokes models.

### 10.1 Urban dispersion modeling: LLNL's Aeolus and CEA's PMSS

Both the LLNL Aeolus and the CEA PSWIFT illustrate the complex pattern of the wind vectors in downtown Chicago and the Paris Opera district. The flow field is influenced both by the characteristics of individual buildings and by the configuration of the city, which differs greatly between Paris and Chicago. Horizontal channeling in street networks is a major effect in the urban environment. The modeling of the vertical flow component seems to also be significant. Both effects pose substantial modeling challenges.

From a global point of view, the flow patterns computed by Aeolus and PSWIFT are not very different, particularly for daytime and nighttime Paris and for daytime Chicago. The major dissimilarity observed is in the vertical velocity component, with Aeolus predicting much broader upward and downward motions than PSWIFT. This is closely related to a large difference in flow modeling approaches allowing Aeolus better capability in capturing and reproducing vertical motion. This difference, specifically, is that Aeolus rigorously solves

the Navier-Stokes equations of the fluid dynamics while PSWIFT uses analytical formulae of the flow field near the buildings and the mass conservation equation.

Both Aeolus and PSPRAY have an LPDM component based on different equations and different turbulence parameterizations (see Annexes A and B). This can introduce differences in the computations by the Lagrangian dispersion models. Moreover, as discussed in the previous paragraph, Aeolus and PSPRAY use significantly different wind and turbulence fields as input data, the driving factor for discrepancy between CEA and LLNL urban dispersion results. The horizontal components and, even more, the vertical component of the wind calculated by Aeolus and PSWIFT induce dissimilarities in the material distribution. This effect is a function of the wind inflow and the size and variability of the buildings and was most clearly observable in the nighttime Chicago case.

## 10.2 Regional dispersion modeling

Regional dispersion was modeled at two levels of meteorological fidelity: (1) lower-fidelity wind single-profile from rawinsonde observations for the Chicago cases; and (2) higher-fidelity 3D gridded WRF weather forecast for both Chicago and Paris cases.

As expected, uniform and constant rawinsonde meteorology results in a simplistic Gaussian type plume for both daytime and the nighttime Chicago cases. The plumes computed by LODI (LLNL/NARAC) and PSPRAY (CEA) propagate in the same direction (to the north at daytime and to the east at nighttime). Concentration contours are similar in length and width, though PSPRAY plumes tend to extend a bit less in the crosswind direction than those of LODI. The total effective dose exceedance levels of 10 and 50 mSv as obtained using LODI and PSPRAY are different. TED contours with SPRAY are smaller in downwind and crosswind directions compared to LODI, a difference warranting further analysis.

The use of vertically and horizontally non-uniform and temporally non-stationary WRF wind forecasts as input meteorology result in a more complex and realistic pattern of radioactive material dispersion, deposition, and dose. In most of the cases in the exercise (Chicago nighttime, Paris daytime and nighttime), WRF-driven plumes do not exhibit a Gaussian shape, being visibly influenced by the wind fields complexity. The concentration contours calculated by LODI and PSPRAY generally agree well both qualitatively and quantitatively. The downwind and crosswind spread of the plumes differs slightly, as dispersion parameters are neither parameterized nor computed in precisely the same

manner. Ultimately, when using WRF 3D wind fields as input meteorology for dispersion computations, the total effective dose predictions obtained by LLNL and CEA are comparable for most cases. The exceedance levels of 10 and 50 mSv contours exhibit a generally consistent yet complex contours associated with (1) meteorological changes (especially in wind direction) and (2) topography, particularly notable for Paris. The consistency of LLNL / NARAC and CEA results for the Chicago and Paris cases, in spite of using different models, is worthy of note and should increase confidence in both sets of models.

## **11 Technical Conclusions: model similarities and discrepancies**

In this table top exercise, LLNL and CEA compared each other's flow and dispersion models. The goal of the comparison was to facilitate the exchange of knowledge, capabilities, and practices, and to demonstrate the utility of modeling dispersal at different levels of computational fidelity. Two scales were examined, a regional scale modeling approach using LPDMs (CEA's PSPRAY and LLNL's LODI), appropriate for simple terrain and/or very large releases, and an urban scale modeling approach (CEA's PMSS and LLNL's Aeolus), appropriate for small releases in a city environment.

At the urban scale, LLNL and CEA used different flow modeling approaches (CEA's PSWIFT employing a simplified diagnostic approach; LLNL's Aeolus employing more rigorous RANS and LES approaches) resulting in distinct 3D flow field and turbulence patterns, and thus in different 3D distribution of the radioactive plume. However, in most cases, the qualitative agreement of the LLNL and CEA concentrations was reasonable. Only the nighttime Chicago case exhibited a more marked discrepancy in the computations, explained by an extremely complex flow configuration (divergence zones). As no measurements were associated to the TTX, it was not possible to draw final conclusions about the performances of the models. However it is quite obvious that full CFD (RANS or LES) should provide a better evaluation of the 3D turbulent flow (especially of the velocity vertical component). The differences between respective LPDMs may also introduce discrepancies in the LLNL and CEA results, though likely minor in comparison to the differences in wind fields.

At the regional scale, LLNL/NARAC and CEA used the same input meteorology, which was of two kinds: (1) single time-varying rawinsondes profiles and (2) WRF wind forecasts. Air concentration prediction contours were generally similar to each other in the Chicago and Paris daytime and nighttime cases. When using a single vertical wind profile, the dose

results (specifically, the exceedance levels of 10 and 50 mSv contours) were somewhat comparable, but CEA's extent of the contours was smaller warranting further analysis. When using WRF time-varying 3D fields, the agreement between LLNL/NARAC and CEA in the exceedance levels of 10 and 50 mSv contours were generally similar for all simulated cases. This comparison is notable, as complicated meteorological situations (terrain complexity and time-varying wind) were associated with most of the simulated cases.

Overall, the regional scale modeling shows a satisfying general agreement while the urban scale modeling would benefit from further in-depth analysis to give a more complete comparison of the capabilities of flow and turbulence models having different levels of fidelity.

## **12 Table Top Exercise Conclusions**

### **12.1 Lessons learned from the exercise**

The TTX exercise provided an excellent opportunity for LLNL and CEA to assess variations in plume model simulation results for different scales and different fidelity, as well as the differential performance of models under different conditions.

Both versions of Aeolus (operated by LLNL) and the PMSS system (operated by CEA) were able to capture important urban phenomena in a timely manner (the TTX lasted three days), such as turbulence regions that might not be identified in a simpler, empirical urban dispersion model. The mass-consistent model modified by buildings flow and the LPDM in PMSS performed quite well, while the fast-running RANS version of Aeolus performed comparably to the more computationally expensive LES model.

Interesting features for the urban cases were not limited to channeling in the street networks, and manifested differently depending on urban environments, sometimes leading to counterintuitive results. For example, while it was anticipated that due to the presence of taller and more varied buildings, vertical dispersion would be higher in Chicago than in Paris, the effect of urban channeling on the plume in Chicago night case highlighted a striking modeling difference. Recall that the night scenario for Chicago involved higher inflow velocities and closer alignment with the street grid than the day case. This caused increased turbulent flow due to wind being diverted down the faces of tall buildings, which in turn reduced street level wind speed. Therefore, higher inflow speed corresponded to reduced dispersal speed. No analogous behavior was observed for Paris, where the streets

do not follow a grid pattern and therefore can never be as aligned with inflowing winds as they can be for Chicago. This particular feature highlights the difficulty in capturing urban dispersal phenomenology using an empirically-based approach, since local effects are influenced by non-local characteristics and are extremely sensitive to meteorological conditions such as atmospheric stability, wind velocity above the urban canopy, and above all, wind direction.

The comparison between single wind profile and high quality 3-D forecast input meteorology for LODI (LLNL/NARAC) and PSPRAY (CEA) was somewhat artificial; locations like Chicago and Paris would likely have data from multiple met stations and time points available in the case of a real emergency. However, highlighting the importance of high quality input data is of interest to LLNL and CEA due to the existence of locations, particularly international locations, where meteorology observations are sparse. At these locations, input similar to the simplified meteorology used here may be all that is available, and would provide an inferior result to a high quality forecast. Therefore, LLNL/NARAC is planning to increase the integration of WRF predictions into operational capabilities, particularly in data sparse regions, while CEA is also going to further develop its capability to operate WRF.

The use of LPDMs at both local and regional scales was a commonality of LLNL and CEA in this exercise. This illustrates the widespread interest in this category of models, which are able to capture the local features of the flow and turbulence and to take account of the buildings (contrary to standard Gaussian models) with low to moderate computational times.

## 12.2 Possible model improvements

This experience suggested several possible improvements to both the exercise format and the underlying models.

For the exercise, model comparisons were limited due to 1) the lack of experimental data for the modeled scenarios and 2) the lack of consistent grids for results from different agencies. Therefore all comparisons were, by necessity, qualitative in nature. The use of shared grids, or interpolation to a shared grid, would allow point-to-point comparison of model output or joint plotting of predictions. However, in the absence of experimental data, even a numerical comparison of models would not indicate which model is more accurate. In keeping with the model validation theme, the incorporation of model uncertainty would also be a necessary step for performing quantitative comparisons.

For specific models, Aeolus would benefit by better incorporating temporally and spatially varying radiological processes (e.g., radiological decay/ingrowth, deposition) and source term models (e.g., stabilized cloud geometries, dynamic cloud rise models) applicable to radiological releases. The resulting radiological CFD model can then be coupled to relevant LLNL geographical, meteorological, and dose conversion factor databases to provide a more complete set of dose and deposition products. As noted in the previous subsection, LODI predictions benefit from the use of high quality, high density meteorology, particularly where weather data is sparse or suspect. This capability is already planned as a future enhancement to the LLNL software.

Regarding the PMSS system, CEA has undertaken the development of PSWIFT-Momentum, which will be a version of PSWIFT resolving the 3D RANS equations for incompressible flow with some simplifying conditions. More specifically, the model is intended to produce a steady state solution for the 3D velocity field on a regular grid. The artificial compressibility method will be used and the turbulence model will certainly be as simple as a zero-equation model along Prandtl's mixing length theory.

In urban configurations, PSPRAY can evaluate the deposition on all exposed surfaces (ground, walls, roofs, etc.) and compute the cloud shine and ground shine taking account of

the shading effects of the buildings. This capability was not used during the TTX as the irradiation computations are quite long. In the near future, the cloud shine and ground shine algorithm will be optimized in order to dramatically diminish the associated computational time.

Recall that, as PMSS is embedded in the more general CERES® CBRN-E modeling and decision support system, it benefits from the dose conversion factors databases and the modules assessing the radiological exposure by the different pathways (inhalation, cloud shine, and ground shine).

Overall this exercise provided valuable insight into both development stage LLNL and CEA modeling capabilities and how best to exercise and assess them. This kind of concentrated assessment effort might make an invaluable addition to LLNL and CEA in the future by giving a preview of future capabilities, as well as guidance for how best to advance such efforts to enhance operations.

### **12.3 Concluding comments on modeling urban releases**

From the TTX, it appears that LLNL and CEA share a common interest in the generation of new flow and dispersion models able to cope with the complex local (built) and regional atmospheric environments. It would be of interest to extend the comparison of Aeolus and PMSS by considering a more systematic sampling of built environments, wind patterns, and release scenarios.

For flow modeling, questions still arise if the simplified CEA model is able to give sufficiently precise results or if it is now time for CEA to shift to RANS with some simplifying assumptions for solutions to turbulent flow problems. From the exercise, LLNL Aeolus-RANS gives results with computation time as short as the diagnostic model in PMSS. While most of the time the PMSS diagnostic model produces satisfying solutions for the flow field, it would be very instructive to compare this model with PSWIFT-Momentum and RANS-Aeolus. Thus, a more systematic benchmark of LLNL and CEA flow models could be arranged on the basis of wind tunnel and / or full scale experimental results.

For dispersion modeling, LLNL and CEA use the same category of LPDMs with differences that could be more deeply analyzed to further understand the consequences of the model parameterizations, and thus explain the potential differences in their results.

The LLNL and CEA meeting also showed that the agencies have common research topics as indoor/outdoor transfers, uncertainty evaluation and source term reconstruction. Although these are currently topics of active research, they will be increasingly relevant in an operational context. Inter-agency exchange on these topics would allow each to benefit from the other's experiences.

Finally, as the agencies agree that this kind of exercise is useful for both LLNL and CEA, it could be advisable to organize future exercises taking account of the lessons learned from this TTX and using real meteorological forecasts over parts of France or the US.

### 13 Acronyms, definitions, and abbreviations

Aeolus	LLNL/NARAC CFD model capable of both RANS and LES
ARAC	LLNL Atmospheric Release Advisory Capability
Bq	Becquerel, the SI derived unit of radioactivity (1 Bq corresponds to 1 decay/second)
CEA	Commissariat à l'Energie Atomique et aux énergies alternatives (FR)
CERES®	CEA modeling and decision-support dedicated to atmospheric dispersion and human health / environment consequences evaluation (the research version of CERES® encompasses PMSS)
Ci	Curie, a non-SI unit of radioactivity, $1 \text{ Ci} = 3.7 \times 10^{10} \text{ Bq}$
Cs-137	Cesium 137, a radioactive isotope associated with radioactive releases
CFD	Computational fluids dynamics
DNS	Direct numerical simulation
DOE	Department of Energy (US)
dx	Grid spacing in x direction (also dy and dz)
FR	France
IAEA	International Atomic Energy Agency
ICRP	International Commission on Radiation Protection
IXP	International Exchange Program (NARAC)
GFS	Global forecast system
k	Von Karman constant
LES	Large eddy simulation
$L_i$	Length of computational grid where $i = x, y$ or $z$
LLNL	Lawrence Livermore National Laboratory
LODI	Lagrangian Operational Dispersion Integrator, the NARAC random-walk dispersion model
LPDM	Lagrangian Particle Dispersion Model
MADIS	Meteorological Assimilation Data Ingest System
NA-40	US Department of Energy's Office of Emergency Operations
NARAC	National Atmospheric Release Advisory Center at LLNL
NNSA	National Nuclear Security Administration (US DOE)
NWP	Numerical weather prediction
PMSS	Parallel-Micro-SWIFT-SPRAY, a modeling system made of PSWIFT (diagnostic flow modeling) and PSPRAY (LPDM), used at CEA

RANS	Reynolds-averaged Navier Stokes
QUIC	Quick Urban & Industrial Complex Dispersion Modeling System, a fast response urban dispersion model developed at Los Alamos National Lab
QUICK	A higher order difference scheme for interpolating advective kinematics
Rawinsonde	An ascending sensor measuring wind speed and direction, temperature, pressure, and humidity
RDD	Radiological dispersal device
rem	A non-SI measurement of dose (100 erg/gram)
Shapefile	A popular data format for geographic information
SOR	Successive over-relaxation method
Sv	Sievert, the SI measurement of dose (J/kg)
TED	Total effective dose (Sv or rem per ICRP Publication 66)
TTX	Table top exercise
u	Wind speed
$u_{ref}$	Reference wind speed at height $z_{ref}$
USA	United States of America (alternately just US)
UTM	Universal Transverse Mercator
WRF	Weather Research Forecast model
$z_0$	Boundary layer height
$z_{ref}$	Reference height for $u_{ref}$

## 14 Acknowledgements

The authors wish to thank Joseph Krol and Vince McClelland of NNSA for suggesting and funding this effort as well as their active participation during the July table top exercise in California. Their insight into what would actually occur during an international urban RDD release was instrumental in framing the scenarios and in analyzing the modeling results. We would also like to thank Megan Daniels, Katie Lundquist, Joe Morris, John Nasstrom, Stephanie Neuscamman, Jim Oldani, Tom Piggott, Brenda Pobanz, and Gayle Sugiyama of LLNL for their participation, assistance, and review of the exercise and of the technical content of this report.

## 15 References

- Baldwin, B. & Lomax, H., 1978. Thin layer approximation and algebraic model for separated turbulent flows. *American Institute of Aeronautics and Astronautics*, p. Vol.257.
- Chen, Q. & Xu, W., 1998. A zero-equation turbulence model for indoor airflow simulation. *Energy and buildings*, Issue 28, pp. 137-144.
- Chorin, A. J., 1968. Numerical solution of the Navier-Stokes equations. *Math Comput.*, Volume 22, pp. 745-762.
- Duchenne, C. et al., 2011. *Application of PMSS, the parallel version of MSS, to the micro-meteorological flow field and deleterious dispersion inside an extended simulation domain covering the whole Paris area*. Kos, Greece, s.n., pp. 679-683.
- Durbin, P., 1983. *Stochastic differential equations and turbulent dispersion*, s.l.: NASA STI/Recon Technical Report N, 83, 22546.
- Eckerman, K. F., 1993. *External exposure to radionuclides in air, water, and soil : exposure-to-dose coefficients for general application, based on the 1987 federal radiation guidance*, s.l.: US EPA, Report EPA 402-R-93-081.
- Eckerman, K. & Leggett, R., 2008. *User Guide to DCFPAK 2.2*, Oak Ridge, TN: Oak Ridge National Laboratory.
- Gowardhan, A. A., Pardyjak, E. R., Senocak, I. & Brown, M. J., 2011. A CFD-based wind solver for an urban fast response transport and dispersion model. *Environ. Fluid Mech.*, 11(5), pp. 439-464.
- Hanna, S. R., Briggs, G. A. & Hosker, R. P., 1982. *Handbook on Atmospheric Diffusion*, Washington, DC: US DOE.
- Hanna, S. et al., 2011. Comparisons of JU2003 observations with four diagnostic urban wind flow and Lagrangian particle dispersion models. *Atmospheric Environment*, pp. 45(24):4073-4081.
- ICRP, 1977. *Recommendations of the ICRP. ICRP Publication 26*, s.l.: Ann. ICRP 1 (3).
- ICRP, 1979. *Limits for Intakes of Radionuclides by Workers. ICRP Publication 30 (Part 1)*, s.l.: Ann. ICRP 2 (3-4).
- ICRP, 1994. *Human Respiratory Tract Model for Radiological Protection. ICRP Publication 66.*, Ann. ICRP 24 (1-3): s.n.
- ICRP, 1995. *Age-dependent Doses to Members of the Public from Intake of Radionuclides - Part 4 Inhalation Dose Coefficients. ICRP Publication 71*, s.l.: Ann. ICRP 25 (3-4).
- Mellor, G. L. & Yamada, T., 1974. A Hierarchy of Turbulence Closure Models for Planetary Boundary Layers.. *J. Atmos Sci.*, pp. 31: 1791-1806.
- Miller, P. A., Barth, M. F. & Benjamin, L. A., 2009. *A 2009 update on NOAA meteorological assimilation data ingest system (MADIS)*. Phoenix, AZ, American Meteorological Society.
- Miller, P. A. et al., 2005. *The meteorological assimilation and data ingest system (MADS): Providing value-added observations to the meteorological community*. Washington, D.C., American Meteorological Society.
- Neophytou, M., Gowardhan, A. & Brown, M., 2011. An inter-comparison of three urban wind models using Oklahoma City Joint Urban 2003 wind field measurements. *Journal of Wind Engineering and Industrial Aerodynamics*, Volume 99, pp. 357-368.
- Oldrini, O., Moussafir, J., Armand, P. & Duchenne, C., 2011. *Development of PMSS, the parallel version of the Micro-SWIFT-SPRAY flow and dispersion in urban environment modelling system*. Kos, Greece, s.n., pp. 443-445.

Prandtl, L., 1926. Application of the “Magnus effect” to the wind propulsion of ships. *NACA TM 387*.

Skamarock, W. C. et al., 2008. *A Description of the Advanced Research WRF Version 3*, s.l.: NCAR Tech Note.

Smith, A. & Cebeci, T., 1967. *Numerical Solution of the Turbulent-boundary-layer Equations*, No. DAC-33735: DOUGLAS AIRCRAFT CO INC LONG BEACH CALIF AIRCRAFT DIV.

Thomson, D. J., 1987. Criteria for the selection of stochastic models of particles trajectories in turbulent flows. *Journal of Fluid Mechanics*, pp. 180:529-556.

Tinarelli, G. et al., 2007. *Micro-Swift-Spray (MSS) a new modelling system for the simulation of dispersion at micro-scale. General description and validation*. s.l., Springer, pp. 449-458.

Tinarelli, G. et al., 2013. *Review and validation of Micro-Spray, a Lagrangian particle model of turbulent dispersion*. s.l., AGU, pp. 200:321-327.

## 16 Circulation of the report

United States – US Department of Energy, Lawrence Livermore National Laboratory

France – Commissariat à l’Energie Atomique et aux énergies alternatives

20 copies

## 17 Appendix A: Details on Aeolus model

### 17.1 Turbulence closure

**RANS.** The Aeolus model can be run very efficiently using a Reynolds Averaged Navier-Stokes model (RANS). The model produces a steady state solution for the 3D velocity field (Gowardhan, et al., 2011). We have opted for one of the simplest approaches to the closure problem, namely, the zero equation model (Baldwin & Lomax, 1978), (Smith & Cebece, 1967). Based on the assumption that there exists an analogy between the action of viscous stresses and Reynolds stresses on the mean flow, a simplified zero equation (algebraic) turbulence model based on Prandtl's mixing length theory was used (Prandtl, 1926).

$$u_T = (l_{mix})^2 \sqrt{S_{ij} S_{ij}}$$

The mixing length  $l_{mix} = ky$ , where  $y$  is the shortest distance to any building wall or ground and  $k$  is the von-Karman constant and  $\overline{S_{ij}} = \frac{1}{2} \frac{\partial \overline{u_i}}{\partial x_j} + \frac{\partial \overline{u_j}}{\partial x_i}$ .

**LES.** The model can be run in a *high fidelity* mode using *Large Eddy Simulation* (LES) model. A simple Smagorinsky model is used:

$$u_T = (c_s D)^2 \sqrt{S_{ij} S_{ij}}$$

Where  $D = \sqrt[3]{dx dy dz}$  and  $\overline{S_{ij}} = \frac{1}{2} \frac{\partial \overline{u_i}}{\partial x_j} + \frac{\partial \overline{u_j}}{\partial x_i}$ .

### 17.2 Dispersion model

To model dispersion within the atmosphere, Aeolus solves the three-dimensional, incompressible, advection- diffusion equation with sources and sinks:

$$\frac{\partial \overline{c}}{\partial t} + \overline{u} \frac{\partial \overline{c}}{\partial x} + \overline{v} \frac{\partial \overline{c}}{\partial y} + \overline{w} \frac{\partial \overline{c}}{\partial z} = \frac{\partial}{\partial x} \left( \overline{c} \eta_x \frac{\partial \overline{c}}{\partial x} \right) + \frac{\partial}{\partial y} \left( \overline{c} \eta_y \frac{\partial \overline{c}}{\partial y} \right) + \frac{\partial}{\partial z} \left( \overline{c} \eta_z \frac{\partial \overline{c}}{\partial z} \right) + Q$$

Where  $\overline{c}$  is the mean air concentration of the species;  $\overline{u}$ ,  $\overline{v}$ , and  $\overline{w}$  are the mean wind components in the  $x$ ,  $y$ , and  $z$  projection directions respectively;  $\eta_i$  is the eddy diffusivity and  $Q$  is the source term.

Aeolus solves stochastic differential equations within a Lagrangian framework (Durbin, 1983). The equations for the particle displacement due to advection, diffusion, and settling in the three coordinate directions are:

$$\begin{aligned} dx &= \bar{u}dt + \frac{\sigma_x n_t}{\sigma_x} dt + (2n_t)^{1/2} dW_x \\ dy &= \bar{v}dt + \frac{\sigma_y n_t}{\sigma_y} dt + (2n_t)^{1/2} dW_y \\ dz &= \bar{w}dt + \frac{\sigma_z n_t}{\sigma_z} dt + (2n_t)^{1/2} dW_z - w_s dt \end{aligned}$$

Where  $dW_{x,y,z}$  are three independent random variates with zero mean and variance  $dt$ . The stochastic differential equations above are then integrated in time to calculate an independent trajectory for each particle. The ensemble-mean concentration, at any time  $t$ , can then be calculated from the particle locations at time  $t$  and the contaminant mass associated with each particle.

The model has been validated against Joint Urban 2003 dataset (Oklahoma City) and Urban 2000 dataset (Salt Lake City).

## 18 Appendix B: Details on PMSS model

### 18.1 Turbulence closure in PSWIFT

PSWIFT implements several formulas to diagnose turbulent fluxes, either with first order closure schemes (Hanna, et al., 1982) or with a second order closure scheme (Mellor & Yamada, 1974).

PSWIFT also has specific turbulence schemes associated with obstacle situations. These can be added to classical formulations seen as background turbulence, such as Hanna's formulation above.

In the Hanna parameterization, the vertical domain is subdivided into three layers:

- S1  $z < h$
- S2  $h < z < h_{\text{res}}$
- S3  $h_{\text{res}} < z < z_{\text{top}}$

Where  $z$  is the height above the ground, while  $z_{\text{top}}$  is the top of domain level. In the case of weaker solar radiation and during night,  $h$  comes to represent the height of the atmospheric neutral or stable boundary layer. The parameter  $h_{\text{res}}$  defines the so-called "height of the residual layer" (Stull, 1988), i.e. the height of the residual turbulent layer developed during the previous day, still existing at night and in the morning above the stable layer. If  $h_{\text{res}}$  is lower than the height of the boundary layer, the S2 layer is absorbed. Inside the first layer S1, profiles are determined as follows, on the basis of the actual stability condition.

Stable conditions  $0 < L_{\text{mo}} < +300$

$$\sigma_1(z) = 2.0 u_* (1 - z/h) \text{ and } \sigma_2(z) = 1.3 u_* (1 - z/h)$$

$$\sigma_u(z) = \sigma_v(z) = \sqrt{0.5 (\sigma_1^2 + \sigma_2^2)}$$

$$\sigma_w(z) = 1.3 u_* (1 - z/h)$$

$$\tau_{Lx}(z) = \tau_{Ly}(z) = 0.11 (h/\sigma_{Ux})(z/h)^{0.5}$$

$$\tau_{Lz}(z) = 0.10 (h/\sigma_w)(z/h)^{0.8}$$

Neutral conditions      $L_{mo} \geq +300$     $L_{mo} \leq -300$

$$\begin{aligned}\sigma_1(z) &= 2.0 u_* e^{(-3 fz/u_*)} \text{ and } \sigma_2(z) = 1.3 u_* e^{(-2 fz/u_*)} \\ \sigma_u(z) = \sigma_v(z) &= \sqrt{0.5 (\sigma_1^2 + \sigma_2^2)} \\ \sigma_w(z) &= 1.3 u_* e^{(-2 fz/u_*)} \\ \tau_{Lx}(z) = \tau_{Ly}(z) = \tau_{Lz}(z) &= 0.5 z / [ \sigma_w (1 + 15 fz/u_*) ]\end{aligned}$$

Unstable conditions      $-300 < L_{mo} < 0$

$$\begin{aligned}\sigma_u(z) = \sigma_v(z) &= u_* (12 - 0.5 h/L_{mo})^{1/3} \\ \sigma_w(z) &= \begin{cases} 0.763 (z/h)^{0.175} & z \leq 0.4h \\ 0.722 w_* (1 - z/h)^{0.207} & 0.4h < z \leq 0.96h \\ 0.37 w_* & 0.96h < z \leq h \end{cases} \\ \tau_{Lx}(z) = \tau_{Ly}(z) &= 0.15 h / \sigma_u \\ \tau_{Lz}(z) &= \begin{cases} 0.1 z / [ \sigma_w (0.55 + 0.38(z - z_0)/L_{mo}) ] & z \leq 0.1h \text{ and } z < z_0 - L_{mo} \\ 0.59 z / \sigma_w & z \leq 0.1h \text{ and } z \geq z_0 - L_{mo} \\ 0.15 (h/\sigma_w) [1 - e^{(-5z/h)}] & z > 0.1h \end{cases}\end{aligned}$$

Inside the S2 layer (when it exists), calculations proceed as in the neutral case, interpolating the equations with the results obtained on the layer below in the region between S1 and S2. In the S3 layer, variances are linearly brought to 0 at the domain top level, whereas Lagrangian time scales are kept constant.

Local formulation is used if obstacles such as buildings are inside the computational domain and is based on a mixing length scheme. The model assumes homogeneity in the equation for the turbulent kinetic energy, denoted  $k$ , to get  $P = \varepsilon$  where  $P$  is the production rate of turbulent kinetic energy and  $\varepsilon$  is its dissipation rate.

The turbulence is modeled introducing the turbulent viscosity  $\nu_t$  which relates the Reynolds stress tensor to the production  $P = 2 \nu_t S_{ij} S_{ij}$ .

As a closure equation for the turbulence, turbulent viscosity is related to a specific mixing length  $L_m$  and the shear of the flow as  $\nu_t = L_m^2 \sqrt{2 S_{ij} S_{ij}}$ , which is derived from the Kolmogorov related hypothesis used in standard  $k$ - $\varepsilon$  models:  $\nu_t = k^2 / \varepsilon$

Several formulations can be used to derive the mixing length from the distance  $L_b$  to the closer solid boundary, either the ground or buildings. The simplest formulation is  $L_m = L_b$ , the mixing length being clipped at a value of 100 m, which is the maximum typical scale of turbulent eddies considered by the turbulence scheme.  $L_m$  is computed, then  $\nu_t$ , then production and dissipation. Finally  $k$  is derived from  $\nu_t$  and dissipation rate  $\varepsilon$ . The diffusive coefficient  $K$  is derived from  $K = \nu_t$  and Lagrangian times from:

$$\sigma_u^2 = \sigma_v^2 = \sigma_w^2 = \sqrt{0.5 K C_0 \varepsilon}$$

$$\tau_{Lu} = \sigma_u^2 / (C_0 \varepsilon)$$

$$\tau_{Lv} = \sigma_v^2 / (C_0 \varepsilon)$$

$$\tau_{Lw} = \sigma_w^2 / (C_0 \varepsilon) \text{ with } C_0 = 2.3$$

## 18.2 Dispersion modeling in PSPRAY

PSPRAY is based on a 3D form of the generalized Langevin equation for the random velocity (Thomson, 1987). The position of each particle  $x_i$ , at each time step, is obtained by numerically integrating the following 3D equations:

$$dx_i = (\bar{u}_{ai} + u_i + u_{bi})dt$$

Where the turbulent velocity  $u_i$  is computed by the following Lagrangian stochastic equation:

$$du_i = a_i(\mathbf{u}, \mathbf{x}, t) dt + b_{ij}(\mathbf{u}, \mathbf{x}, t) dW_j(t)$$

And where  $i, j = 1, 2, 3$ ,  $\bar{u}_{ai}$  is the mean wind velocity vector (whose vertical component is equal to zero in flat terrain only),  $u_{bi}$  is an additional velocity accounting for the buoyancy effects,  $\mathbf{x}$  is the vector of the particle position, and  $\mathbf{u}$  is the Lagrangian velocity vector. The term  $a_i(\mathbf{u}, \mathbf{x}, t)$  is a deterministic term,  $b_{ij}(\mathbf{u}, \mathbf{x}, t) dW_j(t)$  is a stochastic term, and  $dW_j(t)$  is an incremental Wiener process with variance  $dt$ .

The term  $b_{ij}(\mathbf{u}, \mathbf{x}, t)$  is obtained from the Kolmogorov theory of local isotropy in the inertial subrange. Its expression is the following:

$$b_{ij} = \delta_{ij} \sqrt{C_0 \varepsilon}$$

Where  $\delta_{ij}$  is the Kronecker delta,  $\varepsilon$  is the dissipation rate of turbulent kinetic energy, and  $C_0$  is a numerical constant. As an alternative choice, when  $\varepsilon$  is not known or because the value of  $C_0$  is not well established (varying from 2 to 8), it is common to use:

$$b_{ij} = \delta_{ij} \sqrt{\frac{2\sigma_i^2}{T_{Li}}}$$

where  $T_{Li}$  are the Lagrangian decorrelation time scales, and  $\sigma_i^2$  is the velocity fluctuation variance.

The Lagrangian stochastic equation for the turbulent velocity  $u_i$  satisfies the well-mixed condition that particles that are initially uniformly distributed must remain so, which is the criterion for selecting the correct model for the diffusion of scalars in a turbulent flow. Therefore, the term  $a_i(\mathbf{u}, \mathbf{x}, t)$  depends on the Eulerian PDF,  $P(\mathbf{x}, \mathbf{u})$ , of the turbulent velocity, and it is determined from the Fokker-Planck equation:

$$\frac{\partial}{\partial x_i} [u_i(\mathbf{x}, \mathbf{u}) P(\mathbf{x}, \mathbf{u})] = \frac{\partial}{\partial u_i} [a_i(\mathbf{x}, \mathbf{u}) P(\mathbf{x}, \mathbf{u})] + \frac{1}{2} \frac{\partial^2}{\partial u_i \partial u_j} [b_{ij}^2(\mathbf{x}) P(\mathbf{x}, \mathbf{u})]$$

The model has been validated against Joint Urban 2003 dataset (Oklahoma City) (Hanna, et al., 2011).

## 19 Appendix C: Radiological exposure assessment – CEA Method

PMSS simulations provide 3D nuclide concentrations every minute. Output concentration is an average of instantaneous concentration during this minute. Thus, in each point (I, J, K) of the grid, airborne concentration at a time  $t_i$  is equal to:

$$C(I, J, K, t_i) = \frac{\int_{t_{i-1}}^{t_i} C(I, J, K, t) \cdot dt}{\Delta t}$$

Where  $\Delta t = t_{i-1} - t_i = 1$  min.

A rigorous dose assessment would require continuing the simulation until all particles leave the computational domain in order to evaluate the integral of radionuclide concentration. The required condition holds approximately in this case, as only few particles remain inside the grid at the end of simulation ( $t_0 + 30$  min).

Total effective dose (TED) is the sum of three contributions: inhalation, irradiation by the cloud shine, and irradiation by the ground shine (due to deposition).

In each point (I, J) of the grid, the dose by inhalation for a stationary person is modeled as:

$$H_{inh}(I, J) = \left( \sum_{t_i=t_1}^{t_i=t_N} C(I, J, K=1, t_i) \cdot \Delta t \right) \cdot \frac{\tau_{resp}}{3600} \cdot f_{inh} \cdot 1000$$

with:

$H_{inh}(I, J)$	Inhalation dose	mSv
$C(I, J, K=1, t_i)$	Airborne concentration on the first K-level	Bq/m <sup>3</sup>
$\Delta t$	Averaging duration	s
$\tau_{resp}$	Respiration rate (for an adult)	m <sup>3</sup> /h
$f_{inh}$	Effective inhalation dose coefficient	Sv/Bq

The respiration rate for an adult with normal activity is given in ICRP Publication 66 (ICRP, 1994) and is equal to 1.2 m<sup>3</sup>/h. The effective inhalation dose coefficient is given by ICRP Publication 71 (ICRP, 1995) and is equal to 4.6 10<sup>-9</sup> Sv/Bq for Cs-137 (for a 1 μm aerodynamic diameter aerosol, “slow” (S) lung clearance, and exposure of an adult integrated to the age of seventy).

External exposure by the cloud shine for a stationary person is modeled as:

$$H_{\text{irr}}(I, J) = \left( \sum_{t_i=t_1}^{t_i=t_N} C(I, J, K=1, t_i) \cdot \Delta t \right) \cdot f_{\text{irr}} \cdot 1000$$

with:

$H_{\text{irr}}(I, J)$	Radiation dose due to the exposure to the cloud	mSv
$f_{\text{irr}}$	Effective irradiation dose coefficient (cloud shine)	(Sv/s)/(Bq/m <sup>3</sup> )

External exposure due to ground shine is modeled as:

$$H_{\text{dep}}(I, J) = D(I, J, t_{\text{end}}) \cdot f_{\text{dep}} \cdot (\Delta t_{\text{exp}} \cdot 3600) \cdot 1000$$

with:

$H_{\text{dep}}(I, J)$	Radiation dose due to ground deposition	mSv
$f_{\text{dep}}$	Effective irradiation dose coefficient (ground shine)	(Sv/s)/(Bq/m <sup>2</sup> )
$D(I, J, t_{\text{end}})$	Ground deposition once the cloud has gone	Bq/m <sup>2</sup>
$\Delta t_{\text{exp}}$	Duration of the exposure	h

Both radiation dose coefficients for cloud shine and ground shine are given in Federal Guidance 12 (Eckerman, 1993) and are equal to  $2.73 \cdot 10^{-14}$  (Sv/s)/(Bq/m<sup>3</sup>) and  $5.55 \cdot 10^{-16}$  (Sv/s)/(Bq/m<sup>2</sup>), respectively, for Cs-137.

Total effective dose (TED) is obtained by adding the three contributing pathways with the dose due to ground deposition exposure integrated over a four day duration, which is chosen as a typical short-time dose guideline.

## 20 Appendix D: Radiological exposure assessment – LLNL/NARAC Method

LODI simulations provide 3D nuclide concentrations with time. Output concentration can be instantaneous, time-averaged, peak-averaged or integrated. The type of concentration used depends upon the application. Total Effective Dose (TED) calculations make use of time-integrated concentrations and deposition integrated over four days.

The TED is calculated as the sum of four contributing pathways: 1) inhalation of radioactive material from the cloud, 2) external irradiation from the cloud (cloud shine), and 3) irradiation from radioactive material deposited to the surface (ground shine) and 4) inhalation of re-suspended radioactive material previously deposited to the surface.

LODI also keeps track of the decay of radioactive material into daughter products. In this case, Cs-137 was modelled. Cs-137 has a daughter product of Ba-137m. This means that at each time step the concentrations and depositions of both Cs-137 and Ba-137m was calculated. The TEDs calculated therefore must take into account not only all four pathways, but the decay from Cs-137 to Ba-137m and its resulting impact on the dose.

At each point (I, J) of the grid near ground level, the dose due to inhalation for a person who remains in the same location for the entire period is calculated:

$$D_{inh}(I, J) = \int_{t_1}^{t_N} C(I, J, 1, t) dt \cdot BR \cdot DCF_{inh}$$

where:

$D_{inh}(I, J)$	Inhalation dose	rem
$C(I, J, 1, t_i)$	Airborne concentration at 10m agl	Ci/m <sup>3</sup>
BR	Breathing rate (for an adult)	m <sup>3</sup> /s
$DCF_{inh}$	Inhalation dose conversion factor	rem/Ci

The breathing rate for an adult with light exercise is given in ICRP Publication 66 (1993) and is equal to 1.5 m<sup>3</sup>/h. The effective inhalation dose coefficient is given by DCFPAK version 1.8 (2009) and is equal to 1.4504 x 10<sup>5</sup> rem/Ci (3.92 10<sup>-8</sup> Sv/Bq) for Cs-137 (for a 1 µm median aerodynamic diameter aerosol, “slow” (S) lung clearance, and exposure of an adult over a 50-year period following intake of inhaled activity). For inhalation pathway only, this dose factor includes daughter products.

External exposure due to cloud shine for a stationary person is calculated:

$$D_{CS}(I, J) = \left( \int_{t_1}^{t_N} C(I, J, 1, t) dt \right) \cdot DCF_{CS}$$

where:

$D_{CS}(I, J)$	Radiation dose due cloud shine	rem
$C(I, J, 1, t)$	Airborne concentration near ground level	Ci/m <sup>3</sup>
$DCF_{CS}$	Cloud shine dose conversion factor	(rem/s)/(Ci/m <sup>3</sup> )

The cloud shine dose conversion factors were given in DCFPAK version 2.2 (Eckerman & Leggett, 2008) as  $3.48 \times 10^{-4}$  (rem/s)/(Ci/m<sup>3</sup>) [ $9.4 \times 10^{-17}$  (Sv/s)/(Bq/m<sup>3</sup>)] for Cs-137 and  $9.95 \times 10^{-2}$  (rem/s)/(Ci/m<sup>3</sup>) [ $2.69 \times 10^{-14}$  (Sv/s)/(Bq/m<sup>3</sup>)] for Ba-137m.

External exposure due to ground shine is calculated:

$$D_{GS}(I, J) = \int_{t_1}^{t_N} Dep(I, J, t) dt \cdot DCF_{GS} \cdot GRF$$

where:

$D_{GS}(I, J)$	Radiation dose due to ground shine	rem
$DCF_{GS}$	Ground shine dose conversion factor	(rem/s)/(Ci/m <sup>2</sup> )
$Dep(I, J, t)$	Deposition on the surface	Ci/m <sup>2</sup>
GRF	Ground roughness factor	-

The ground roughness factor represents shielding of deposited material by other surrounding material on the ground. The dose conversion factors for ground shine are given in DCFPAK version 2.2. The ground shine dose factor for Cs-137 is  $1.16 \times 10^{-5}$  (rem/s)/(Ci/m<sup>2</sup>) [ $2.85 \times 10^{-19}$  (Sv/s)/(Bq/m<sup>2</sup>)]. Additionally the ground shine dose conversion factor for Cs-137's daughter, Ba-137m is  $2.13 \times 10^{-3}$  (rem/s)/(Ci/m<sup>2</sup>) [ $5.86 \times 10^{-16}$  (Sv/s)/(Bq/m<sup>2</sup>)].

Internal exposure due to inhalation of re-suspended radioactive material is calculated:

$$D_{re}(I, J) = \int_{t_1}^{t_N} Dep(I, J, t) dt \cdot S_f \cdot BR \cdot DCF_{inh}$$

where:

$D_{re}(I,J)$	Dose due to inhalation of re-suspended radioactive material	rem
$Dep(I,J,t)$	Deposition to the surface	Ci/m <sup>2</sup>
BR	Breathing rate (for an adult)	m <sup>3</sup> /s
$DCF_{inh}$	Inhalation dose conversion factor	rem/Ci
$S_f$	Re-suspension factor	m <sup>-1</sup>

The re-suspension factor varies with time according to the following method:

$$S_f = 10^{-5} \exp[-0.07(t-t_{dep})] + 7 \times 10^{-9} \exp[-0.002(t-t_{dep})] + 10^{-9}$$

where  $t_{dep}$  represents the time of deposition (days) and  $t$  has units of days.

TED is obtained by adding the four contributing pathways that have been integrated over a four day duration, which is chosen as a typical short-term dose guideline.